Melanoma drug discovery: Prioritization of candidate melanoma driver mutations in the ErbB4 receptor tyrosine kinase gene and identification of novel molecules that disrupt ErbB4 signaling

by

Richard Lee Cullum

A dissertation submitted to the Graduate Faculty of
Auburn University
in partial fulfillment of the
requirements for the Degree of
Doctor of Philosophy

Auburn, Alabama
May 2, 2020

Keywords: ErbB4, melanoma, targeted therapy, receptor mediated phenomena, cancer drug discovery, high-throughput screening

Copyright 2020 by Richard Lee Cullum

Approved by

Allan E. David, Co-Chair, Associate Professor of Chemical Engineering
David J. Riese II, Co-Chair, Professor of Drug Discovery and Development
Elizabeth A. Lipke, Associate Professor of Chemical Engineering
Maria L. Auad, Professor of Chemical Engineering

Abstract

BRAF V600E mutations are found in roughly 50% of metastatic melanomas. While these tumors typically initially respond to BRAF and/or MEK inhibitors, they frequently develop resistance to BRAF and/or MEK inhibition. Fortunately, the five-year survival for metastatic melanoma has improved to approximately 50%, in part, due to the contribution of anti-CTLA-4, -PD-1, and -PD-L1 immunomodulators [1-7]. However, there are still no effective targeted therapies against metastatic melanomas that do not harbor the *BRAF* V600E driver mutation. Thus, there is a pressing need for additional biomarkers and actionable targets in metastatic melanoma.

In this work, analyses of The Cancer Genome Atlas (TCGA) Skin Cutaneous Melanoma (SKCM) clinical melanoma genomic data set revealed that a significant fraction of melanomas (14%) harbor at least one mutation in the gene that encodes for the ErbB4 receptor tyrosine kinase. However, unlike the validated melanoma oncogene *BRAF*, no single *ERBB4* mutation was predominant among the melanoma genomes. Instead, there were 71 unique *ERBB4* nonsynonymous missense mutations. Here, various *in silico* approaches were used to prioritize *ERBB4* nonsynonymous missense mutations in melanoma on their likelihood to function as melanoma drivers. The results of these analyses suggest that many of the *ERBB4* mutations in the TCGA-SKCM data set are likely to contribute to the malignant phenotype of melanoma. Therefore, there remains a need to determine which *ERBB4* mutations are *bona fide* drivers of melanoma cell

proliferation. The results of this work will serve as a platform for the characterization of putative *ERBB4* driver mutations in melanoma.

Since it appears that a significant fraction of melanoma patients likely harbor driver mutations in *ERBB4*, there is a need for the development of therapeutics that disrupt ErbB4 signaling. As a result, in this work, a drug discovery strategy was developed based on the observation that the Q43L mutant of the naturally occurring ErbB4 agonist NRG2β functions as a partial agonist at ErbB4. NRG2β/Q43L stimulates tyrosine phosphorylation, fails to stimulate ErbB4-dependent cell proliferation, and inhibits agonist-induced ErbB4-dependent cell proliferation. Molecules that exhibit these characteristics are likely to function as ErbB4 partial agonists, and as such hold promise as therapies for the treatment of ErbB4-dependent melanomas. Consequently, three highly sensitive and reproducible ($Z' > 0.5$) semi-automated screening assays were developed and deployed for the identification of small-molecules that function as partial agonists at ErbB4. As a result, six small-molecules were identified that stimulate ErbB4-phosphorylation, fail to stimulate ErbB4-dependent cell proliferation, and appear to selectively inhibit ErbB4-dependent cell proliferation. Therefore, these molecules could potentially function as ErbB4 partial agonists and have potential as therapies against ErbB4-dependent melanomas. While further characterization and optimization is required to evaluate the full therapeutic potential of these molecules, the platform on which they were identified certainly demonstrates reliable and scalable approaches for the discovery of ErbB4 inhibitors.

Acknowledgments

I would first like to thank my advisors, Dr. Allan David and Dr. David Riese, for all of their support and guidance throughout my graduate studies. I would like to also thank Dr. Ram Gupta for his guidance during my first two years at Auburn. That being said, thank you, Dr. David, for letting me join your lab upon Dr. Gupta's departure and constantly supporting my pursuit of research that I am truly passionate about. And, thank you, Dr. Riese, for the endless hours spent discussing research progress, experimental design, and career development. Most importantly, thank you so much for introducing me to the world of cancer drug discovery. I am extremely grateful for the time each of you invested as I pursued my work at Auburn.

I would also like to thank my committee members, Dr. Elizabeth Lipke and Dr. Maria Auad, for their time and expertise. In addition, I would like to thank Dr. Bruce Smith for serving as the outside reader for my dissertation. I would also like to thank all of the former members of the Gupta Lab and all of the current and past members of the David and Riese Labs for being great coworkers and friends. And, a huge thank you to my team of undergrads that helped me keep the Riese Lab running smoothly when I was the only graduate student in the group: Tyler Piazza, Logan Neel, and Jared Senfeld. I would not have been nearly as productive without the help from each of you. I am also unbelievably thankful for the family of friends that I have made while at Auburn. Thank

you for all of the tailgates, football and baseball games, festivals, crawfish boils, and just being an invaluable support system.

Finally, I would like to thank my family for always being there and their never-ending support. Thank you to my parents, Bill and Dana Cullum, and siblings, Bill Jr. and Tracy, for always showing interest in what I am up to in the lab and your constant encouragement throughout all of my academic studies. And, lastly, I would like to thank my wife, Deborah Michelle Cullum, for all of her love and support as my time at Auburn comes to an end and we embark on our next great adventure.

Additionally, this work would not have been possible without the support from a US Department of Education GAANN Graduate Fellowship Program in Biological and Pharmaceutical Engineering (Award No. P200A120244 to Auburn University) and an Auburn University Research Initiative in Cancer (AURIC) Graduate Fellowship in Cancer Research.

Table of Contents

List of Tables

List of Figures

List of Abbreviations

ATCC	American Type Culture Collection
AU	absorbance units
β-gal	beta-galactosidase
BaF3	mouse pro-B-lymphocyte cell line
BRAF	BRAF member of RAF proteins
BRAF	human gene that encodes BRAF protein
BSA	bovine serum albumin
CEM	human T-lymphoblastoid cell line
CTLA-4	cytotoxic T-lymphocyte-associated protein 4
EC_{50}	drug concentration that gives half-maximal response
EGF	epidermal growth factor
EGFR	epidermal growth factor receptor tyrosine kinase
EGFR	gene that encodes for EGFR receptor tyrosine kinase
ELISA	enzyme-linked immunosorbent assay
E_{max}	maximum efficacy of a dosed drug
ErbB	ErbB family of receptor tyrosine kinases
ERBB	genes that encode for the ErbB family of receptor tyrosine kinases
ErbB1	a.k.a. EGFR
ErbB2	receptor tyrosine kinase ErbB2

ERBB2	gene that encodes for the ErbB2 receptor tyrosine kinase
ErbB3	receptor tyrosine kinase ErbB3
ERBB3	gene that encodes for the ErbB3 receptor tyrosine kinase
ErbB4	receptor tyrosine kinase ErbB4
ERBB4	gene that encodes for the ErbB4 receptor tyrosine kinase
FDA	US Food and Drug Administration
HEK 293T	human embryonic kidney 293 cell line with SV40 T-antigen
HER2	a.k.a. ErbB2
HER3	a.k.a. ErbB3
HER4	a.k.a. ErbB4
HRAS	gene that encodes for the HRAS protein
HRP	horseradish peroxidase
IC_{50}	inhibitor concentration that reduces response by half
IL3	interleukin 3
I_{max}	maximum inhibitory effect of dosed drug
KRAS	gene that encodes for the KRAS protein
MAPK	mitogen-activated protein kinase
MEK	MAPK/ERK kinase
MTT	3-(4, 5-dimethylthiazolyl-2)-2, 5-diphenyltetrazolium bromide
NCI	National Cancer Institute
Neu	a.k.a. ErbB2
NF1	gene that encodes for the NF1 protein
NIH 3T3	mouse embryonic fibroblast cell line

NRAS	NRAS member of RAS proteins
NRAS	gene that encodes for the NRAS protein
NRG1β	neuregulin 1beta
NRG2β	neuregulin 2beta
PBS	phosphate-buffered saline
PD-1	programmed cell death protein 1
PD-L1	programmed death ligand 1
PI3K	phosphoinositide 3-kinase
QSAR	quantitative structure-activity relationship
RAF	RAF kinase family
RAS	RAS protein family
RPMI	Roswell Park Memorial Institute
RTK	receptor tyrosine kinase
SH2	Src Homology 2
shRNA	short hairpin RNA
SKCM	skin cutaneous melanoma
TCGA	The Cancer Genome Atlas

Chapter 1: Introduction

1.1. Metastatic melanoma

Melanoma is an aggressive form of skin cancer that originates in melanocytes. Melanocytes, which are melanin-producing cells that reside in the basal layer of the epidermis, primarily serve as protection against ultraviolet radiation. However, uncontrollable growth of melanocytes can lead to the formation of melanoma. While not the most common type of skin cancer, melanoma is the most fatal[8]. Fortunately, most cases are diagnosed when the melanoma is still a localized disease. Localized melanoma can typically be surgically removed and patients have about a 98% 5-year survival rate[8]. Unfortunately, many patients are not diagnosed with melanoma during the early stages of the disease. In many cases, melanoma remains undiagnosed until the melanoma cells have spread through the lymph nodes to distant sites in the body. At this point, the disease is referred to as metastatic melanoma, or Stage IV melanoma. Patients that are diagnosed with metastatic melanoma currently have a 5-year survival rate of about 50%[1-7].

1.2. Current treatment strategies for metastatic melanoma

Unlike localized melanoma, metastatic melanomas cannot be eradicated by surgical excision alone. Until the last decade, treatment of patients with metastatic melanoma was limited to radiation and chemotherapy to eradicate metastases that could not be removed by excision. Due to a better understanding of the biological

underpinnings that lead to melanoma genesis and progression, several targeted therapies have recently been developed for patients with metastatic melanoma. For one, it was observed that about 90% of melanomas exhibit elevated activation of the RAS/RAF/MEK/MAPK pathway[9]. This led to the discovery that about 50% of melanoma tumors contain a genetic alteration in the gene that encodes the BRAF protein and about 20% of melanomas harbor a mutation in the gene that encodes the NRAS protein. The identification of these mutations drove the development and FDA approval of BRAF inhibitors, such as vemurafenib in 2011, and MEK inhibitors, such as trametinib in 2013, for patients harboring a V600E mutation in *BRAF*[10-12]. While the clinical results of these therapies were initially promising, the duration of response has been heavily limited by the development of resistance mechanisms to the inhibitors when used as monotherapies and in combination[9].

An increase in the understanding of the immune regulation of T-cells has also been imperative in the development of better therapies for patients with metastatic melanoma. Elevated levels of immune checkpoint proteins such as PD-L1 allow the melanoma tumor cells to effectively "turn off" the T-cell's immune response against the tumor cells. This discovery led to the development and FDA approval of immune checkpoint therapies such as PD-1 inhibitors (pembrolizumab, 2014) and CTLA-4 inhibitors (ipilimumab, 2011) for patients with metastatic melanoma[13,14]. These immunotherapies have yielded promising results as monotherapies and in combination with BRAF and MEK inhibitors leading to a drastic change in the standard-of-care treatment strategy for metastatic melanoma patients[9].

1.3. Current clinical problem

Despite the major improvements that have been made in the standard-of-care treatment of metastatic melanoma as a result of targeted therapies and immunotherapies, there still remains a significant clinical issue. There are still no effective targeted therapies against metastatic melanomas that do not harbor the *BRAF* V600E driver mutation. Thus, there is a pressing need for additional biomarkers and actionable targets in metastatic melanoma.

1.4. Overarching dissertation goals

Therefore, the two overarching goals for this dissertation project were: (1) to prioritize *ERBB4* mutants that are likely to function as drivers of melanoma tumor cell proliferation and (2) to develop a drug screening strategy to identify molecules that disrupt ErbB4 signaling.

1.5. Contributions to the field

To address the first goal, a systematic *in silico* workflow was developed and implemented for the prioritization of candidate melanoma driver mutations in the ErbB4 receptor tyrosine kinase gene. This is the first in-depth analysis of clinically-relevant *ERBB4* mutations in melanoma using The Cancer Genome Atlas (TCGA) melanoma genomic data set. Moreover, the results of this work will serve as a platform for future wet-lab efforts to identify which *ERBB4* mutations contribute to melanoma tumorigenesis and progression.

To address the second goal, a semi-automated screening process was developed and deployed for the identification of small-molecule compounds that function as ErbB4 partial agonists. The screening process can now be used by others in the field for the identification of molecules that stimulate or disrupt ErbB4 signaling. The small-molecule compounds that were identified to disrupt ErbB4 signaling in this work have therapeutic potential for a significant fraction of melanoma patients. Furthermore, the molecules identified in this work have the potential for being the first selective inhibitors of ErbB4.

The details of the work that was completed in order to make these contributions are described in the remaining chapters of this dissertation. Chapter 2 focuses on the prediction of putative melanoma driver mutations in *ERBB4*, and Chapter 3 focuses of the identification of novel molecules that disrupt ErbB4 signaling. The overall conclusions of this dissertation will be discussed in Chapter 4, and the future directions for the work within this dissertation will be covered in Chapter 5.

1.6. The drug discovery and development continuum

The drug discovery and development continuum can be divided into three main stages: preclinical, clinical, and commercialization. The focus of this dissertation lies in the preclinical phases of anticancer drug discovery and development. The preclinical phases typically include: (1) Target identification and validation, (2) Model system development, (3) Screening assay development and hit identification, (4) Hit validation, and (5) Lead candidate development. More specifically, this work focuses on (1) Target identification and (3) Screening assay development and hit identification.

1.6.1. Modern target identification

The advances in technology and decreasing costs of genomic sequencing and high-throughput systems has led to a large growth of datasets available for drug discovery. Furthermore, open data initiatives such as the NCI Genomic Data Commons [15] and the cBioPortal [16,17] have allowed the general public to have access to real clinical datasets to improve drug discovery efforts. The types of data that are stored in these disease-specific datasets include gene expression, protein expression, single-nucleotide polymorphisms (SNPs), copy number variations (CNVs), drug-target interaction, patient survival data, pathology reports, diagnostic/tissue/radiological imaging, and several other forms of clinical data.

Researchers frequently use these large datasets to identify novel drug targets and biomarkers. In cancer drug discovery, specifically, researchers commonly use datasets containing sequenced tumor genomes to identify potential driver genes that caused the tumor cells to have a growth-advantage. The identification of BRAF V600 mutations in melanoma and the subsequent development of BRAF inhibitors was one the first successful examples of using genomics for drug discovery [12,18-20]. In fact, this example set a precedent for the development of modern targeted chemotherapies.

Although these data sets have led to the development of therapies for novel targets, they have also allowed for the repurposing of existing therapeutics. For example, the identification of *KIT* as a gastrointestinal stromal tumor target allowed for the repurposing of the KIT inhibitor, imatinib, which was originally used to treat myelogenous leukemia [21].

1.6.2. High-throughput screening for hit identification

Advances in combinatorial chemistry, genomics, proteomics, and bioinformatics has greatly increased the size of screening compound libraries. As a result, HTS (high-throughput screening) platforms were developed to sort through the large libraries of potential drug molecules. In fact, over the last 20 years, HTS has become a standard platform for early stage drug discovery in the pharmaceutical industry. Furthermore, it was the needs of HTS labs that initiated many of the advances in laboratory automation, assay miniaturization, data capture, and assay formats [22]. While HTS does provide methods necessary for screening collections of up to 500,000 compounds, it also provides a relatively unbiased approach for identifying novel drug molecules [23].

HTS assays generally fall into one of two categories, biochemical assays and cell-based assays. Biochemical assays detect and often quantify the binding affinity of molecules to a target or the biological activity of the target. These assays provide insight to the mechanism of action of a potential drug compound. Cell-based assays provide biological information about how an organism will respond to a given compound. These assays allow for the determination of cell viability, proliferation, and cytotoxicity after treatment with a potential drug molecule.

Some examples of successful chemotherapies that were identified using HTS drug discovery technologies are the FDA-approved tyrosine kinase inhibitors gefitinib, erlotinib, sorafenib, dasatinib, and lapatinib [22]. Although HTS assays are powerful tools for the discovery of new therapies, their implementation is rather resource intensive. Assay development and validation alone is time consuming and requires a lot of optimizing to be fit for the screening of large libraries of compounds. Successful

optimization of HTS assays is paramount considering the screening costs for a 500,000-compound library can cost anywhere between $250,000 - $500,000 [24]. Building and maintaining the chemical compound library is also extremely expensive in terms of personnel, space, and equipment. The deployment of the screens is also time-consuming and requires the investment of expensive laboratory automation such as liquid handlers. The large amounts of data generated by HTS efforts also take a lot of time to analyze to identify the most promising hits.

1.7. Bridging chemical engineering and cancer drug discovery

In the era of big data and precision medicine, cancer drug discovery is no longer predominately pursued by life scientists. Instead, teams of life scientists, mathematicians, physicists, chemists, and engineers are all necessary to successfully complete the preclinical phases of the current drug discovery and development continuum. Mathematicians commonly utilize their training to develop complex algorithms to sort through large omics datasets for target discovery. Life scientists, then, utilize their training to validate newly identified targets via wet lab experiments. Physicists and chemists use their skills to develop libraries of synthetic drug molecules that are likely to specifically bind to the desired drug target. Engineers, especially chemical engineers, utilize their skills for the development of processes for the identification and production of novel drug molecules, as well as develop novel strategies for drug delivery.

Since chemical engineering focuses on chemical and biological transformations and the systems in which these transformations occur [25], developing processes to identify novel drug molecules that harbor specific biochemical and biological

characteristics is well within the skillsets of a chemical engineer. Just as any chemical process, developing scalable and reproducible drug discovery processes requires the use of many chemical engineering principles such as thermodynamics, reaction kinetics, and process design/optimization.

1.7.1. Thermodynamics in drug discovery

The industry standard for discovering "hit" molecules that hold potential as drug molecules involves the use of high-throughput screening (HTS) assays to screen large libraries of small molecule compounds or monoclonal antibodies. The development of high-throughput screening assays involves practical application of chemical thermodynamics. Since HTS assays are performed on microplates (96 wells/plate, 384 wells/plate, and 1536 wells/plate), a major challenge is minimizing well-to-well and plate-to-plate variability. Under optimal conditions, each well on each plate will experience identical environmental and reaction conditions at all times. Therefore, all automated protocols must be scripted such that each well is treated in the same manner for the same amount of time on every plate. If not, the screens will undoubtedly display plate-effects in which the background signal is not consistent across the plate(s). Inconsistent background signal levels can lead to the selection of false positives or the culling of false negatives when deploying the screen.

Outside of maintaining balanced automated scripts, the conditions of each well on each plate must remain identical during incubation periods in-between the automated steps of screens. If not properly controlled for, the reaction conditions of the wells around the edges of the plates can quickly become different from the inner wells. This is simply

due to a relative humidity gradient on the plate. The relative humidity is highest at the center of the plate and lowest at the edges where the wells are not surrounded by other wells full of solution. As a result, the solvent evaporation rate is higher at the edges which causes the concentration of reactants in the well to increase and the equilibrium of the reaction to be shifted. Examples of controlling the relative humidity to maintain reaction equilibria include using adhesive plate seals during overnight incubation steps, and the use of a humid environment to reduce solvent evaporation around the edges of plates.

1.7.2. Reaction kinetics in drug discovery

Several aspects of drug discovery require an understanding reaction kinetics. Fortunately, reaction kinetics is at the core of fundamental chemical engineering training. Often, in cancer drug discovery, it is ideal to identify a molecule that inhibits the function of a target that is providing a growth-advantage to cancer cells. In this case, cell-based and biochemical assays are developed for the identification of molecules that function as inhibitors at a desired target. The development of reliable and reproducible assays is heavily dependent upon a complete understanding of the reaction kinetics throughout the assay. This knowledge can be used to alter reaction times and temperatures as well as reagent concentrations to optimize the assay for HTS use.

Interpreting the results of HTS campaigns also requires the use of reaction kinetics. Especially in the case of using the results of cell-based assays to determine the mechanism-of-action for “hit” molecules. A classic example of this is determining whether a molecule is functioning as a competitive or noncompetitive inhibitor (**Figure**

1). Since a competitive inhibitor binds to the same location as the substrate, it is understandable that large amounts of substrate can overcome the effect of the inhibitor and vice versa. Therefore, in cellular proliferation assays, competitive inhibition can be identified by a shift in the EC_{50} of the substrate and the recovery of maximal proliferation using an excess of substrate (**Figure 1**). Since a noncompetitive inhibitor does not bind to the same site as the substrate, the substrate, regardless of concentration, will never be able to overcome the effect of the inhibitor. Furthermore, the inhibitor will never be able to completely overcome the effect of the substrate. Consequently, noncompetitive inhibitors exhibit no effect on the substrate EC_{50} but reduce the maximal effect of the substrate (**Figure 1**).

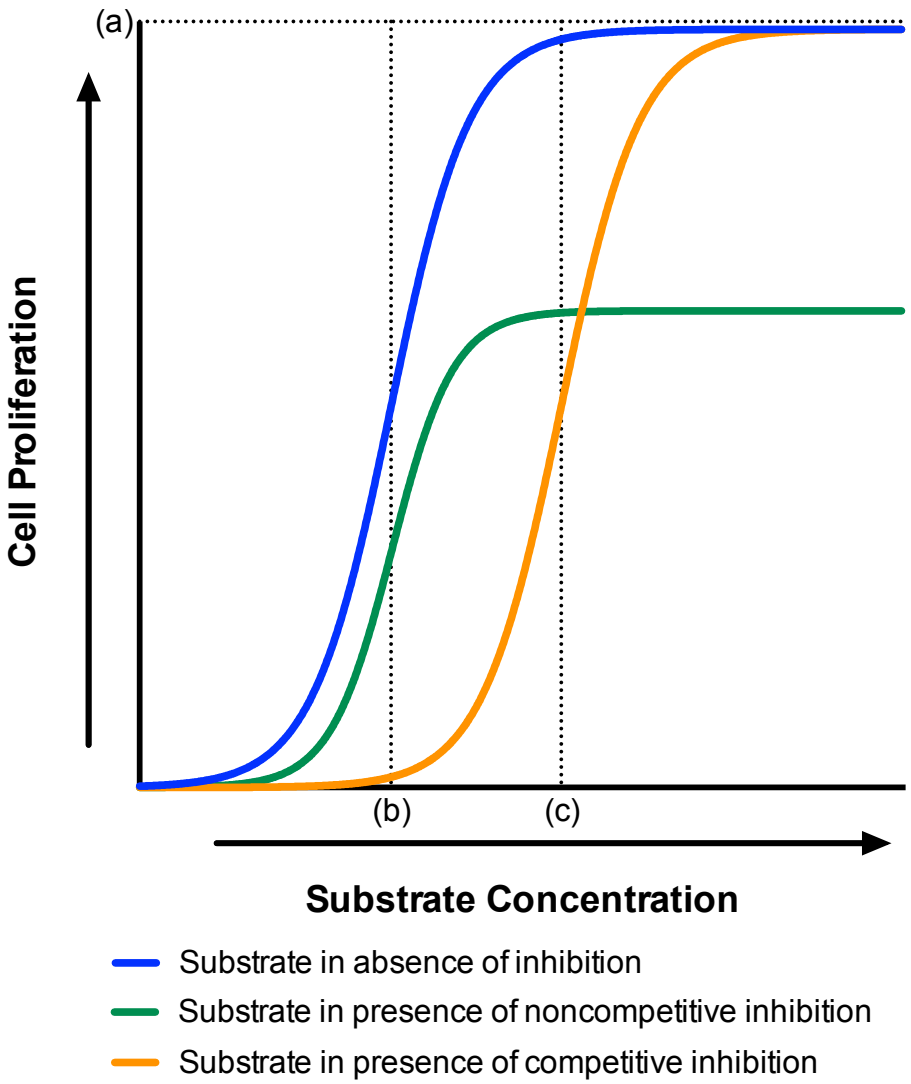

Figure 1. Cellular proliferation as a function of substrate concentration. (a) E_{max}; Maximal cellular proliferation stimulated by the substrate in absence of inhibition. (b) EC_{50} (substrate concentration at which cellular proliferation is 50% of maximal cell proliferation stimulated by the substrate) for no inhibition and noncompetitive inhibition. (c) EC_{50} for competitive inhibition.

1.7.3. Process design in drug discovery

HTS assays must be designed and developed such that they can be scaled to accommodate various library sizes. The order in which the screens are deployed is also imperative so that screening campaigns can quickly identify the most promising

candidates. While chemical engineers do focus optimizing biological and chemical transformations, they also focus on developing scalable systems to produce desired products. Although drug discovery HTS processes are not traditional chemical engineering processes, the skill sets attained from chemical engineering training are easily adapted for developing effective drug discovery platforms. In fact, designing an HTS process is conceptually similar to distillation; a process chemical engineers are very familiar with. Similar to the multicomponent feedstock entering a distillation column, an HTS process begins with a large library of unique chemical compounds. The engineer is tasked with developing a process using screening assays (unit operations) that filters and selects for the desired product.

In the case of this dissertation, a process needed to be developed for identifying inhibitors of cell proliferation stimulated by the ErbB4 receptor tyrosine kinase. Furthermore, the inhibitor must also partially activate the receptor by stimulating tyrosine phosphorylation of the receptor. Given this scenario, three HTS assays were used to identify molecules that stimulate ErbB4 tyrosine phosphorylation, fail to stimulate ErbB4-dependent cellular proliferation, and specifically inhibit ErbB4-dependent cellular proliferation. Since the assay to identify ErbB4 tyrosine phosphorylation had the shortest run time (highest throughput), it was utilized as the primary screen in the campaign. This enabled quick evaluation of the entire small-molecule library for a characteristic that was unique to the desired drug mechanism-of-action. To verify that none of the compounds that stimulated ErbB4 tyrosine phosphorylation also stimulated cell growth, the primary assay was followed up with a cell proliferation assay that could detect stimulation of ErbB4-dependent cellular proliferation. Then, compounds that were identified to

stimulate phosphorylation and not stimulate cell proliferation, were screened using another cell proliferation assay to determine whether or not they could specifically inhibit ErbB4-dependent cell proliferation. The effectiveness of deploying the screens in this order is evident in that none of the waste streams (compounds that did not pass a given screen) were recycled back into the screening process (**Figure 18**). Once a compound failed a test, it never had to be retested at a subsequent stage.

As with any process design, measures must be put in place to monitor the performance of the individual screens within the HTS process. HTS facilities have developed rigorous quality control methods such as Z-trend monitoring, plate pattern recognition algorithms, regular usage of pharmacological standards, and liquid handler and reader performance monitoring. In this work, the Z-factor (See Chapter 3) was used as the primary indicator of assay performance during the HTS campaign. Plate pattern recognition and liquid handler and reader performance was evaluated during the developmental stage of the screening assays.

Chapter 2: *In silico* prioritization of candidate melanoma driver mutations in the ErbB4 receptor tyrosine kinase gene

2.1. Introduction

BRAF V600E mutations are found in roughly 50% of metastatic melanomas. While these tumors typically initially respond to BRAF and/or MEK inhibitors, they frequently develop resistance to BRAF and/or MEK inhibition. Fortunately, the five-year survival for metastatic melanoma has improved to approximately 50%, in part, due to the contribution of anti-CTLA-4, -PD-1, and -PD-L1 immunomodulators [1-7]. However, there are still no effective targeted therapies against metastatic melanomas that do not harbor the *BRAF* V600E driver mutation. Thus, there is a pressing need for additional biomarkers and actionable targets in metastatic melanoma.

Here, we have analyzed the TCGA skin cutaneous melanoma (SKCM) genome dataset in effort to identify a potential target/biomarker for these *BRAF* wild-type (WT) tumors. As a result, we believe that *ERBB4* mutant alleles function as biomarkers and drivers in *BRAF* WT melanomas by either (1) increasing the growth stimulatory activity of ERBB4-EGFR heterodimers or by (2) disrupting the growth inhibitory activity of ERBB4 homodimers.

2.2. Results

2.2.1. The incidence of *ERBB4* melanoma missense mutations suggests they are functionally significant

ERBB4 encodes the ErbB4 (HER4) receptor tyrosine kinase and is a member of the ErbB family of receptor tyrosine kinases, a family that also includes the epidermal growth factor receptor (EGFR/ErbB1), ErbB2 (HER2/Neu), and ErbB3 (HER3). In The Cancer Genome Atlas Skin Cutaneous Melanoma (TCGA-SKCM) dataset, 14% of the melanoma genomes harbor at least one nonsynonymous missense mutation in *ERBB4* (**Table 1**).

Table 1. Nonsynonymous missense mutation incidence and N/S (nonsynonymous-to-synonymous) mutation ratios for all ERBB genes in the TCGA-SKCM dataset.

Gene	% of cases with a nonsynonymous missense mutation	N/S
EGFR	6	1.4
ERBB2	3	1.2
ERBB3	2	1.0
ERBB4	14	2.9

This incidence exceeds that of *EGFR* (6%), *ERBB2* (3%), and *ERBB3* (2%) in the same dataset (**Table 1**). Moreover, *ERBB4* is the only *ERBB* gene in the TCGA-SKCM dataset to have a ratio of nonsynonymous to synonymous mutations (N/S) that exceeds the 2.5:1 ratio indicative of driver mutations [26,27]. This suggests that these ERBB4 mutant

alleles are *bona fide* melanoma drivers. In contrast to what is observed with most tumor driver alleles, including the BRAF V600E melanoma driver [28], *ERBB4* mutations in melanoma do not cluster at a predominant "hot spot". Instead, the *ERBB4* mutations found in melanoma are found throughout the entire ErbB4 coding sequence (**Figure 2**).

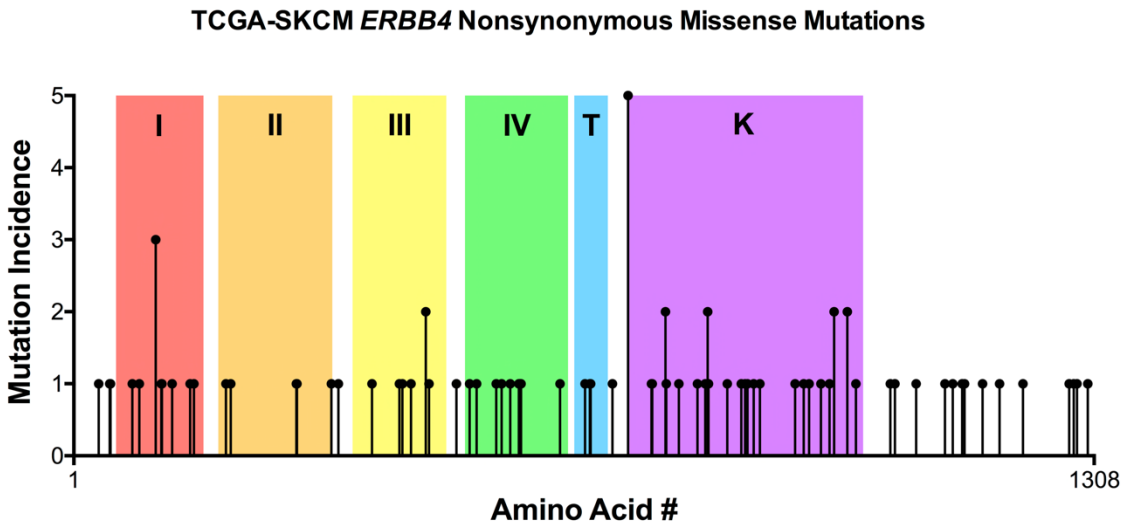

Figure 2. Lollipop plot of *ERBB4* nonsynonymous missense mutations in the TCGA-SKCM dataset. The functional regions of the receptor have been highlighted. The extracellular subdomains I, II, III, and IV are highlighted in red, orange, yellow, and green respectively. The transmembrane domain (T) is highlighted in blue. The intracellular kinase domain (K) is highlighted purple. Mutation incidence (# of TCGA-SKCM cases) is reported on the y-axis.

2.2.2. Sites of *ERBB4* melanoma missense mutations are conserved in other ErbB receptors

2.2.2.1. ERBB4 missense mutations affect residues conserved in EGFR, ErbB2, or ErbB3

Next, we aligned the ERBB4 amino acid sequence with that of each of the other ERBB family receptors. Each of the TCGA-SKCM *ERBB4* mutations were then mapped onto the alignments. This reveals that 49 of the 71 *ERBB4* missense mutations in the TCGA-SKCM dataset affect a residue that is conserved in *EGFR*, *ERBB2*, or *ERBB3* (**Figure 3**).

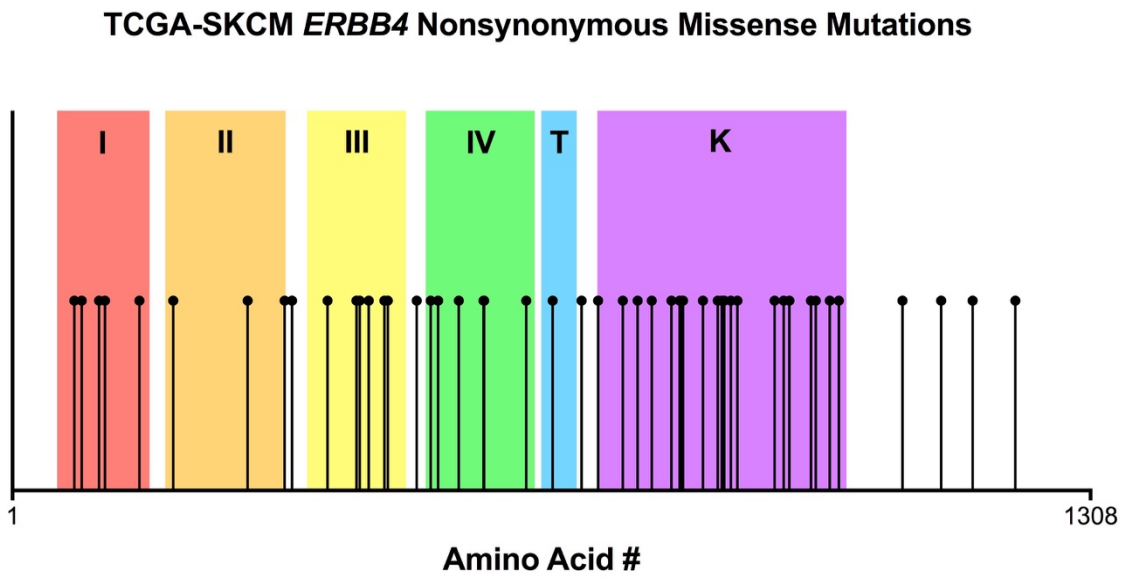

Figure 3. Lollipop plot of TCGA-SKCM *ERBB4* nonsynonymous missense mutations that affect a residue that is conserved in either *EGFR*, *ERBB2*, or *ERBB3*.

2.2.2.2. Sites of ERBB4 mutations are conserved in the region encoding EGFR kinase activity

Given that EGFR and ERBB4 can transphosphorylate EGFR, we predicted that *ERBB4* mutations are more common among ERBB4 residues that are conserved in EGFR. This overrepresentation of *ERBB4* mutations would suggest that the *ERBB4* mutant alleles are functionally significant and are *bona fide* melanoma drivers.

Indeed, chi-squared analysis reveals that codons in *ERBB4* that are conserved in *EGFR* are not more likely to be mutated in the TCGA-SKCM dataset than are *ERBB4* codons that are not conserved in *EGFR* (**Figure 4**, p=0.067). However, codons in *ERBB4* that are conserved in the portion of *EGFR* that encodes the tyrosine kinase domain are significantly more likely to be mutated in the TCGA-SKCM dataset than are codons in *ERBB4* that are not conserved in the portion of *EGFR* that encodes the tyrosine kinase domain (**Figure 4**, p=0.014). Again, these data suggest that *ERBB4* mutant alleles contribute to melanoma genesis or progression.

	All ErbB4 Codons		
	Site of Mutation	Not Site of Mutation	
ErbB4 aa Identical to EGFR	40	609	649
ErbB4 aa Not Identical to EGFR	26	633	659
	66	1242	1308

p=0.067

	ErbB4 Codons in Kinase Domain (aa 710-1012)		
	Site of Mutation	Not Site of Mutation	
ErbB4 aa Identical to EGFR	21	218	239
ErbB4 aa Not Identical to EGFR	0	64	64
	21	282	303

p=0.014

Figure 4. (Left panel) Chi-squared analysis of mutant status of all ErbB4 codons against ErbB4 amino acid conservation with EGFR status. (Right panel) Chi-squared analysis of mutant status of ErbB4 codons in the kinase domain against ErbB4 amino acid conservation with EGFR status.

2.2.2.3. Sites of ERBB4 mutations are conserved in the region encoding the ERBB3 ligand-binding domains

A few EGFR ligands also bind ERBB4, whereas ERBB2 does not bind to any known EGF family ligand. In contrast, numerous ERBB4 ligands also bind ERBB3. Thus, we predicted that *ERBB4* mutations are more common among ERBB4 residues that are conserved in the ERBB3 ligand binding domains (LBDs) than in the EGFR or ERBB2 LBDs. This overrepresentation of *ERBB4* mutations suggests that the *ERBB4* mutant alleles are functionally significant and are *bona fide* melanoma drivers.

Chi-squared analysis indicates that codons in *ERBB4* that are conserved in the *EGFR* or *ERBB2* LBDs are NOT more likely to be mutated in the TCGA-SKCM dataset than are *ERBB4* codons that are not conserved in the *EGFR* or *ERBB2* LBDs. However, codons in *ERBB4* that are conserved in the *ERBB3* LBDs are slightly (but not significantly) more likely to be mutated in the TCGA-SKCM dataset than are *ERBB4* codons that are not conserved in the *ERBB3* LBDs (**Figure 5**, p=0.135). This slight overrepresentation of *ERBB4* mutations is consistent with our hypothesis that the *ERBB4* mutant alleles are functionally significant and are *bona fide* melanoma drivers.

ErbB4 Codons in LBDs (aa 55-634)

	Site of Mutation	Not Site of Mutation	
ErbB4 aa Identical to EGFR	14	272	286
ErbB4 aa not Identical to EGFR	13	281	294
	27	553	580

p=0.787

ErbB4 Codons in LBDs (aa 55-634)

	Site of Mutation	Not Site of Mutation	
ErbB4 aa Identical to ErbB2	12	250	262
ErbB4 aa not Identical to ErbB2	15	303	318
	27	553	580

p=0.938

ErbB4 Codons in LBDs (aa 55-634)

	Site of Mutation	Not Site of Mutation	
ErbB4 aa Identical to ErbB3	20	330	350
ErbB4 aa not Identical to ErbB3	7	223	230
	27	553	580

p=0.135

Figure 5. Chi-squared analysis of mutant status of ErbB4 codons in the ligand binding domains against ErbB4 amino acid conservation with EGFR, ErbB2, and ErbB3.

2.2.2.4. Sites of ERBB4 mutations correspond to sites of driver mutations in EGFR and ERBB2

ERBB4 mutant alleles found in the TCGA-SKCM dataset correspond to driver mutations in *EGFR* or *ERBB2*, suggesting that these *ERBB4* mutant alleles are functionally significant and are *bona fide* melanoma drivers (**Figure 6**). For example, the *ERBB4* R106C and G741E/R mutations each affect ERBB4 residues that are conserved in *EGFR* and are the location of driver mutations in the *EGFR* gene (*EGFR* R108K [29,30] and G735S [31,32]). The *ERBB4* G286V/R mutations correspond to a site of a known driver mutation in the *ERBB2* gene (*ERBB2* G929R [33]). Finally, the *ERBB4* E810K and L864P mutations correspond to sites of known driver mutations in both *EGFR* (*EGFR*

E804G [32] and *EGFR* L858Q/R (aka L834R) [34-37]) and *ERBB2* (*ERBB2* E812K [38] and L866M [39]).

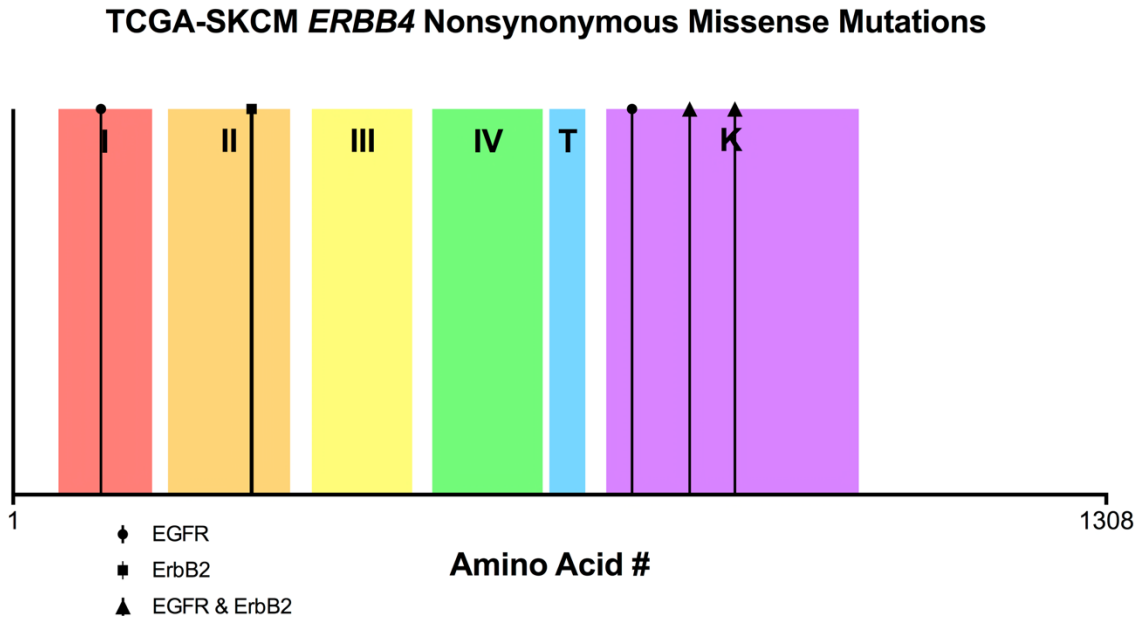

Figure 6. Lollipop plot of the 5 *ERBB4* mutation sites that correspond to sites of driver mutations in *EGFR* or *ERBB2*.

2.2.3. Some of the ERBB4 melanoma missense mutations are found more than once

2.2.3.1. Seven of the 71 ERBB4 melanoma missense mutations are found in more than one TCGA melanoma sample

Whereas most of the *ERBB4* missense alleles in the TCGA-SKCM dataset are unique and occur in only one tumor sample, five of the *ERBB4* missense alleles occur twice in the TCGA-SKCM dataset (E452K, P579L, D813N, S975L, R992C), one occurs three times (R106C), and one occurs five times (R711C) (**Figure 7**). We tested the

hypothesis that these recurrences are due to selection rather than chance by simulating the random assignment of 82 missense mutations to the 1308 codons of *ERBB4*. In 100,000 random assignments, the incidence of a mutation occurring at the same codon twice, three times, or five times is markedly lower than the observed incidence (data not shown), suggesting that *ERBB4* mutant alleles found in metastatic melanomas are not chance occurrences, but are instead the result of selection.

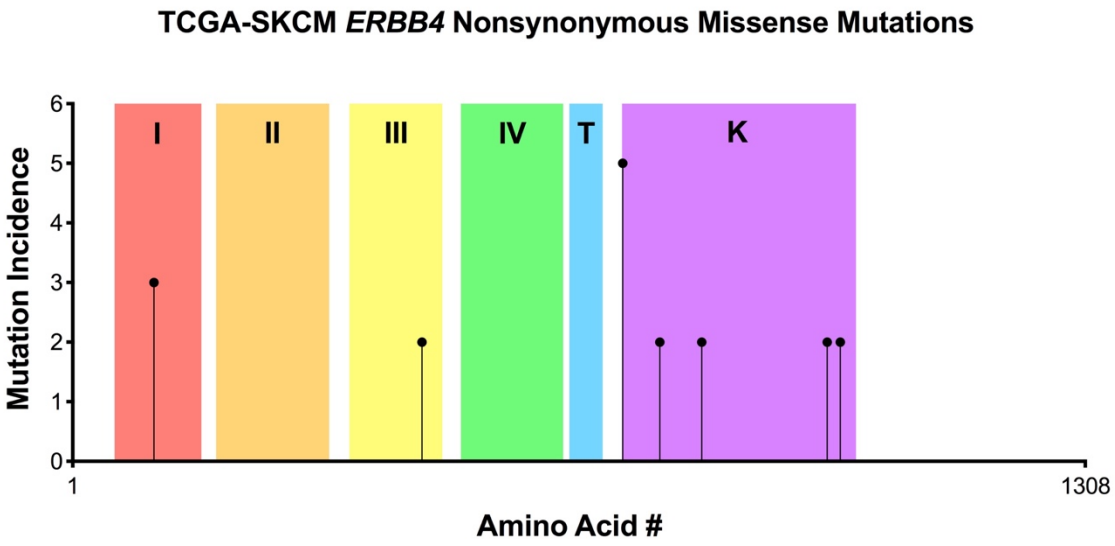

Figure 7. Lollipop plot of the 7 *ERBB4* mutations the are found in more than one TCGA-SKCM sample.

2.2.3.2. 9 of the 71 ERBB4 melanoma missense mutations are found in samples of other types of tumors

Nine of the TCGA-SKCM *ERBB4* missense mutations are found in samples of other tumor types (**Figure 8**) [16,17]. *ERBB4* R106C is found in colorectal adenocarcinoma, pancreatic adenocarcinoma, stomach adenocarcinoma, bladder adenocarcinoma, and skin adnexal carcinoma. *ERBB4* R114Q is also found in colorectal adenocarcinoma. *ERBB4* R196C is found in stomach adenocarcinoma and pancreatic adenocarcinoma. *ERBB4* T4221 and G573D are found in head and neck squamous cell carcinoma. *ERBB4* P572L is found in uterine endometrioid carcinoma. *ERBB4* R711C is found in both invasive breast carcinoma and uterine endometrioid carcinoma. *ERBB4* R838Q is found in colorectal adenocarcinoma and uterine serous carcinoma/uterine papillary serous carcinoma. *ERBB4* R992C is found in uterine endometrioid carcinoma, upper tract urothelial carcinoma, and colorectal adenocarcinoma. These additional occurrences of *ERBB4* mutant alleles suggest that *ERBB4* mutant alleles are bona fide melanoma drivers and that these alleles function as drivers in additional types of tumors.

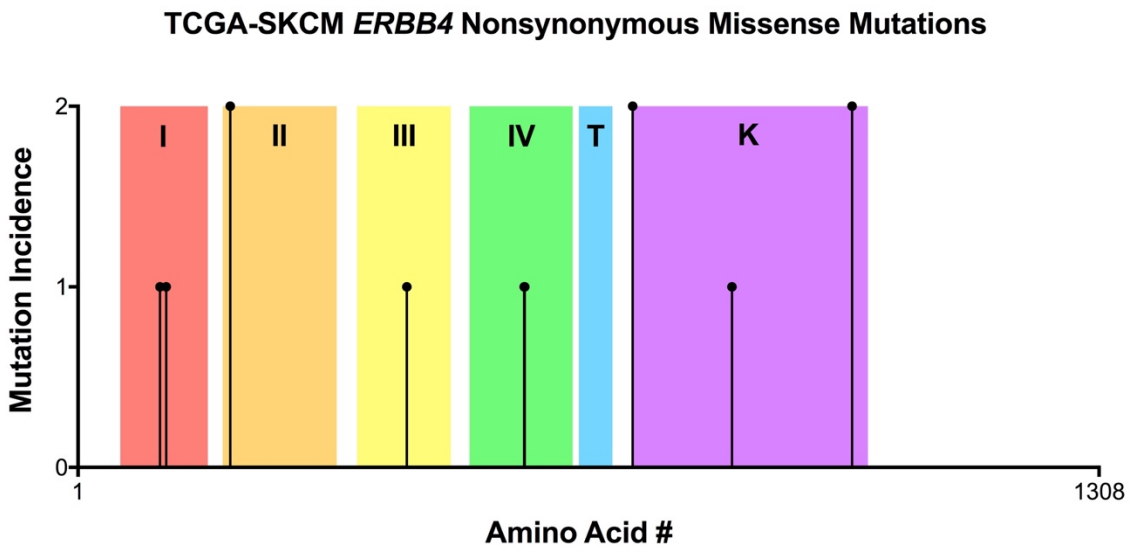

Figure 8. Lollipop plot of the 9 TCGA-SKCM ERBB4 mutations that are found in samples of other tumor types.

2.2.4. The coincidence of ERBB4 melanoma missense mutations with other genetic/epigenetic changes suggests how ERBB4 mutations drive melanoma tumor proliferation

2.2.4.1. The incidence of ERBB4 missense mutations in melanomas is strongly elevated in tumors that have driver mutations in RAS or NF1 genes

As noted earlier, it is well established that ERBB4 can directly stimulate the PI3K signaling pathway. However, the evidence that ERBB4 can stimulate RAS signaling is much weaker than the evidence that EGFR and ERBB2 can stimulate RAS signaling[40]. Therefore, we have indirectly evaluated the hypothesis that ERBB4 is coupled to RAS signaling by measuring the incidence of *ERBB4* mutant alleles in melanoma samples that do or do not possess driver mutations in the *NRAS, KRAS, HRAS,* and *NF1* genes [41,42]. If ERBB4 is directly coupled to RAS signaling in melanoma, then the incidence of

ERBB4 mutant alleles should be inversely correlated with the incidence of driver mutations in the *NRAS*, *KRAS*, *HRAS*, or *NF1* genes.

Surprisingly, the incidence of ERBB4 mutant alleles is ELEVATED in melanomas that possess driver mutations in the *NRAS*, *KRAS*, *HRAS*, or *NF1* genes (p=0.001, chi-squared, **Figure 9**). This coincidence suggests that ERBB4 does not stimulate RAS signaling and that some melanomas are dependent on the cooperation of deregulated ERBB4 signaling with elevated RAS signaling. Moreover, the *ERBB4* missense alleles that coincide with *RAS* or *NF1* driver alleles are better candidate drivers of melanoma than the *ERBB4* missense alleles that are not coincident with *RAS* or *NF1* driver alleles.

Mutations	No Putative Driver Mutation(s) in *NRAS, KRAS, HRAS* or *NF1*	Putative Driver Mutation(s) in *NRAS, KRAS, HRAS* or *NF1*	Total
Missense Mutation in *ERBB4*	28	38	66
No Missense Mutation in *ERBB4*	254	145	399
Total	282	183	465

P = 0.001, Chi-squared

Figure 9. Chi-squared analysis of TCGA-SKCM cases comparing *ERBB4* missense mutation status against putative driver mutation status of *NRAS*, *KRAS*, *HRAS*, or *NF1*.

2.2.4.2. ERBB4 melanoma missense mutations are associated with decreased survival, particularly in the context of a driver mutation in RAS or NF1 genes

Using the TCGA-SKCM dataset, we have analyzed the effects of *ERBB4*, *RAS*, and *NF1* mutant alleles on the survival of 205 melanoma cases (**Figure 10**). Survival is markedly decreased in cases that harbor a combination of *ERBB4* and *RAS* mutant alleles or *ERBB4* and *NF1* mutant alleles relative to cases that do not harbor one of these combinations. Thus, these data support the hypothesis that *ERBB4* mutant alleles cooperate with elevated RAS signaling to drive melanoma aggressiveness.

Mutations	Putative Driver Mutation(s) in a *RAS* gene	Putative Driver Mutation(s) in *NF1*	No Putative Driver Mutation(s) in *RAS* or *NF1*	Total
Missense Mutation in *ERBB4*	1538 days n=9	728 days n=5	2701 days n=10	1854 days n=24
No Missense Mutation in *ERBB4*	2174 days n=48	1721 days n=18	1685 days n=115	1818 days n=181
Total	2074 days n=57	1505 days n=23	1766 days n=125	1822 days n=205

Figure 10. Analysis of all TCGA-SKCM cases that provided days to death data. Reported values are average days to death for cases in the varying mutational circumstances. Total number of cases per circumstance is also included.

2.2.4.3. The incidence of ERBB4 missense mutations in melanoma is markedly reduced in melanoma cases that harbor driver events in the PI3KCA or PTEN genes

We have previously shown that the PI3K pathway mediates ERBB4 coupling to cell proliferation in a heterologous model system (**Figure 11**). If the PI3K pathway mediates ERBB4 coupling to proliferation in melanoma, then we would expect that the incidence of *ERBB4* mutant alleles is inversely correlated with the incidence of other genetic/epigenetic events that stimulate PI3K signaling. (We presume that only a single genetic/epigenetic event – in *ERBB4* or elsewhere - is required to stimulate PI3K signaling.) There are several mechanisms by which PI3K signaling can be stimulated. PI3KCA expression and/or *PI3KCA* copy number can be elevated or gain-of-function *PI3KCA* driver mutations can stimulate PI3K signaling. Furthermore, because the PTEN tumor suppressor protein [43] functions by inhibiting signaling of the PI3K pathway, increased PI3K signaling can result from reduced PTEN expression and/or *PTEN* copy number.

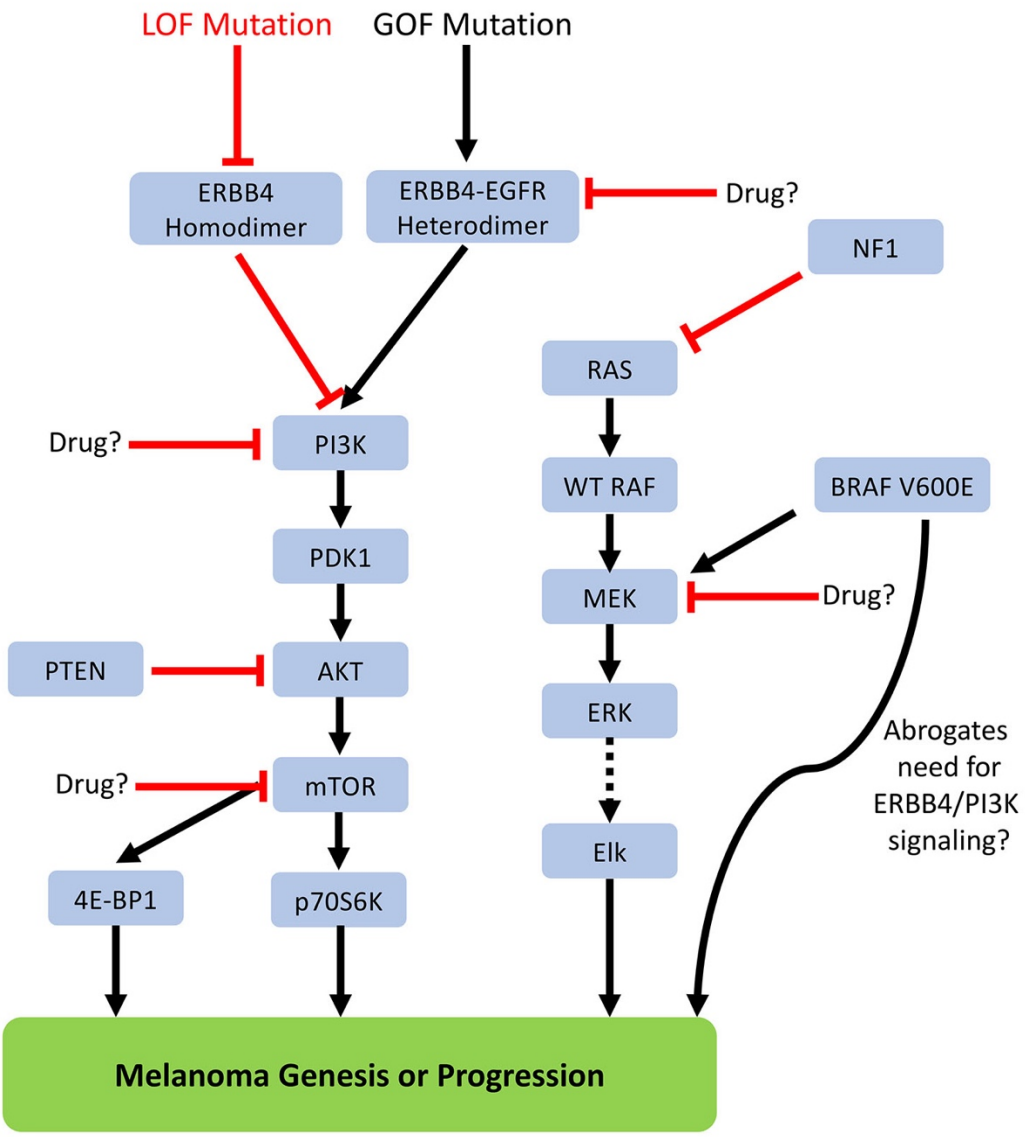

Figure 11. Model for signaling by *ERBB4* mutants.

Thus, metastatic melanoma cases from the TCGA-SKCM dataset were sorted into those cases that possess these driver events in the *PI3KCA* or *PTEN* genes and those cases that do not. The incidence of *ERBB4* mutant alleles in these two groups was determined. This analysis revealed that *ERBB4* mutant alleles are significantly less common in those samples that possess driver events in the *PI3KCA* or *PTEN* genes

(p=0.005, chi-squared, **Figure 12**). This suggests that *ERBB4* mutant alleles are coupled to elevated PI3K signaling. Moreover, the *ERBB4* missense alleles that do not coincide with *PI3KCA* or *PTEN* driver events are better candidate drivers of melanoma than the *ERBB4* missense alleles that are coincident with *PI3KCA* or *PTEN* driver events.

	***ERBB4* WT**	***ERBB4* Mutant**	**Total**
Evidence that signaling by the PI3K/Akt pathway is elevated	183	18	201
NO evidence that signaling by the PI3K/Akt pathway is elevated	217	48	265
Total	400	66	466

P = 0.005

Figure 12. Chi-squared analysis of TCGA-SKCM cases comparing *ERBB4* missense mutation status against evidence of elevated PI3K/Akt pathway signaling.

2.2.4.4. In WT ERBB4 samples, elevated ERBB4 expression is associated with elevated EGFR expression

We and others have previously demonstrated that ERBB4 may function as a homodimer or as a heterodimer with another ERBB receptor [40,44-48]. Moreover, ERBB4-EGFR and ERBB4-ERBB2 heterodimers are oncoproteins whereas ERBB4 homodimers are commonly tumor suppressors[45,47]. To gain insights into whether *ERBB4* mutations found in melanoma samples affect the activity of hetrerodimeric ERBB4 oncoproteins or homodimeric ERBB4 tumor suppressors, we have evaluated the

coincidence of wild-type (WT) *ERBB4* transcription with either *EGFR* transcription or *ERBB2* transcription.

	Elevated *ERBB4 Expression*	Mid-Low *ERBB4* Expression	Total Cases
Elevated *EGFR* Expression	25	45	70
Mid-Low *EGFR* Expression	40	205	245
Total Cases	65	250	315

P = 0.00041

	Elevated *ERBB4 Expression*	Mid-Low *ERBB4* Expression	Total Cases
Elevated *ERBB2* Expression	18	50	68
Mid-Low *ERBB2* Expression	47	200	247
Total Cases	65	250	315

P = 0.179

Figure 13. Chi-squared analysis of the coincidence of wild-type (WT) ERBB4 transcription with either EGFR transcription (left panel) or ERBB2 transcription (right panel) for TCGA-SKCM cases reporting both *ERBB4* and *EGFR* or *ERBB*4 and *ERBB2* expression levels.

This analysis showed that elevated WT *ERBB4* transcription is strongly associated with elevated *EGFR* transcription (P=0.00041, chi-squared, **Figure 13**) but is not significantly associated with elevated *ERBB2* expression (P=0.179, chi-squared, **Figure 13**). This finding suggests that ERBB4 may exist as homodimers in some melanoma samples and as heterodimers in other melanoma samples. Moreover, it appears that ERBB4-EGFR heterodimers may be more important to the genesis and/or progression of melanomas than are ERBB4-ERBB2 heterodimers.

2.2.4.5. In samples of metastatic melanoma and other tumors, ERBB4 copy number is decreased more commonly than increased

As mentioned earlier, ERBB4 homodimers can function as tumor suppressors. Indeed, synthetic constitutively-homodimerized and –active *ERBB4* mutants inhibit the proliferation of many human tumor cell lines [49]. And, elevated ErbB4 expression has been associated with more favorable outcomes in human breast cancers [45].

Protein Name	Gene Name	TCGA Overall % SSM Cases	TCGA Overall +CNV/-CNV	TCGA-SKCM % SSM Cases	TCGA-SKCM +CNV/-CNV
ErbB4	***ERBB4***	**5.8%**	**0.43**	**22.0%**	**0.61**
Tumor Suppressors					
p53	*TP53*	39.3%	0.29	16.0%	0.00
Rb	*RB1*	4.9%	0.18	4.3%	0.23
PTEN	*PTEN*	9.9%	0.21	10.0%	0.19
Oncogenes					
PI3K	*PIK3CA*	13.8%	6.80	3.2%	1.00
B-Raf	*BRAF*	8.0%	1.08	52.2%	4.15
K-Ras	*KRAS*	8.2%	2.85	2.3%	6.00
Abl	*ABL1*	2.4%	1.31	5.5%	2.83

Figure 14. Analysis of average copy number variation (CNV) in *ERBB4,* known tumor suppressor genes, and known oncogenes in both the TCGA-SKCM dataset and the full TCGA dataset including all tumor types. The highlighted values show a significant shift towards evidence of either oncogenic or tumor suppressor function.

ERBB4 copy number variation was analyzed in the TCGA-SKCM dataset as well as across the entire TCGA database (**Figure 14**). As controls, we analyzed copy number variation of known tumor suppressor genes (TP53, RB1, PTEN) and oncogenes (PIK3CA, BRAF, KRAS, ABL1). For each sample, we report the ratio (+CNV/-CNV) of the number of samples that exhibit hyperploidy (copy number >2) divided by the number of samples that exhibit hypoploidy (copy number <2). A ratio of greater than 1 is indicative of a hyperploid oncogene whereas a ratio of less than 1 is indicative of a hypoploid tumor suppressor gene. Indeed, the known tumor suppressors (*TP53*, *RB1*, and *PTEN*) all exhibit a ratio of less than 0.30 in the TCGA-SKCM dataset and in the TCGA overall. Likewise, the known oncogenes *BRAF*, *KRAS*, and *ABL1* all exhibit a ratio of greater than 2.5 in the TCGA-SKCM dataset and the known oncogenes *PIK3CA* and *KRAS* exhibit a ratio of greater than 2.5 in the TCGA overall.

ERBB4 exhibits a ratio of 0.61 in the TCGA-SKCM dataset and 0.43 in the TCGA overall. These results suggest that *ERBB4* is more likely to function as a tumor suppressor gene than as an oncogene in a particular tumor sample. However, in a population of tumor samples, one would anticipate a meaningful fraction of samples in which *ERBB4* functions as an oncogene.

2.2.5. Combining these criteria allows the 71 ERBB4 mutants to be prioritized

2.2.5.1. Each of the 71 ERBB4 mutants can be assigned a priority score

The TCGA-SKCM dataset contains 71 distinct ERBB4 mutants. Taking in all the analysis performed, we believe that it is possible to prioritize them in order of most likely

to functionally alter ErbB4 to least likely. The prioritization scheme presented here was designed to minimally discriminate against *ERBB4* mutants by function. Some high priority mutations, when expressed in metastatic melanoma, may act in a gain-of-function way by increasing chance of heterodimerization or in a loss-of-function way by limiting homodimerization.

The prioritization scheme combines 7 categories (**Table 2**) based on information presented here that when analyzed across the TCGA-SKCM dataset, revealed putative drivers. Each category, if satisfied, earned one point toward the mutation's prioritization status. Any mutant with greater than 4 points was indicated as a high priority mutant (**Table 3**). Any mutant with 4 points is medium-high priority (**Table 3**). Any mutant with 3 points is medium (**Table 3**), 2 points is medium-low (**Table 4**), 1 point is low (**Table 4**), and 0 points are no priority (**Table 4**).

Table 2. TCGA-SKCM *ERBB4* mutant prioritization criteria.

a	Mutation at site conserved in Tyrosine Kinase Domain of EGFR
b	Mutation at site conserved in Extracellular Domains I-IV of ErbB3
c	At site of a driver mutation in EGFR and/or ErbB2
d	Found in a sample of a tumor other than Melanoma
e	Found more than once in TCGA-SKCM data set
f	coincides with a *RAS* and/or *NF1* driver
g	Associated with no evidence of activating alterations in PI3K signaling pathway

Table 3. High, medium high, and medium priority *ERBB4* mutants.

Mutation	a	b	c	d	e	f	g	Priority score	Priority Rating
R106C	-	1	1	1	1	1	1	6	high
R711C	1	-	-	1	1	1	1	5	high
R992C	1	-	-	1	1	1	1	5	high
T422I	-	1	-	1	-	1	1	4	medium high
E452K	-	1	-	-	1	1	1	4	medium high
P759L	1	-	-	-	1	1	1	4	medium high
D813N	1	-	-	-	1	1	1	4	medium high
G85S	-	1	-	-	-	1	1	3	medium
R196C	-	1	-	1	-	-	1	3	medium
P331S	-	1	-	-	-	1	1	3	medium
S418F	-	1	-	-	-	1	1	3	medium
P517A	-	1	-	-	-	1	1	3	medium
P572L	-	-	-	1	-	1	1	3	medium
G573S	-	1	-	1	-	-	1	3	medium
G624W	-	1	-	-	-	1	1	3	medium
G741E	1	-	1	-	-	-	1	3	medium
P800L	1	-	-	-	-	1	1	3	medium
E810K	1	-	1	-	-	-	1	3	medium
R838Q	1	-	-	1	-	-	1	3	medium
D861N	1	-	-	-	-	1	1	3	medium
E872K	1	-	-	-	-	1	1	3	medium
G880R	1	-	-	-	-	1	1	3	medium
P925S	1	-	-	-	-	1	1	3	medium
G936E	1	-	-	-	-	1	1	3	medium
E969K	1	-	-	-	-	1	1	3	medium
S975L	1	-	-	-	1	-	1	3	medium
G286R	-	1	1	-	-	-	1	3	medium
G286V	-	1	1	-	-	-	1	3	medium

Table 4. Medium low, low, and none priority *ERBB4* mutants.

Mutation	a	b	c	d	e	f	g	Priority score	Priority Rating
E33K	-	-	-	-	-	1	1	2	medium low
A48D	-	-	-	-	-	1	1	2	medium low
F76L	-	1	-	-	-	-	1	2	medium low
D113N	-	-	-	-	-	1	1	2	medium low
L155F	-	1	-	-	-	-	1	2	medium low
A383T	-	1	-	-	-	1	-	2	medium low
S433P	-	1	-	-	-	-	1	2	medium low
R491K	-	1	-	-	-	1	-	2	medium low
E542K	-	1	-	-	-	1	-	2	medium low
G549S	-	-	-	-	-	1	1	2	medium low
E560K	-	-	-	-	-	1	1	2	medium low
G741R	1	-	1	-	-	-	-	2	medium low
P759S	1	-	-	-	-	-	1	2	medium low
D776N	1	-	-	-	-	1	-	2	medium low
H856Y	1	-	-	-	-	-	1	2	medium low
L864P	1	-	1	-	-	-	-	2	medium low
P943S	1	-	-	-	-	-	1	2	medium low
P1080L	-	-	-	-	-	1	1	2	medium low
P1117L	-	-	-	-	-	1	1	2	medium low
R1127K	-	-	-	-	-	1	1	2	medium low
R1139Q	-	-	-	-	-	1	1	2	medium low
R1142Q	-	-	-	-	-	1	1	2	medium low
P1165L	-	-	-	-	-	1	1	2	medium low
E1187D	-	-	-	-	-	1	1	2	medium low
G1217E	-	-	-	-	-	1	1	2	medium low
P1276S	-	-	-	-	-	1	1	2	medium low
P1282S	-	-	-	-	-	1	1	2	medium low
R114Q	-	-	-	1	-	-	-	1	low
D150N	-	-	-	-	-	1	-	1	low
G340E	-	1	-	-	-	-	-	1	low
G456E	-	1	-	-	-	-	-	1	low
S508F	-	1	-	-	-	-	-	1	low
P572S	-	-	-	-	-	1	-	1	low
G656E	-	-	-	-	-	-	1	1	low
F662L	-	-	-	-	-	1	-	1	low
E691K	-	-	-	-	-	-	1	1	low
N814T	1	-	-	-	-	-	-	1	low
F1003I	1	-	-	-	-	-	-	1	low
P1300S	-	-	-	-	-	1	-	1	low
G127E	-	-	-	-	-	-	-	0	none
F662V	-	-	-	-	-	-	-	0	none
E1047K	-	-	-	-	-	-	-	0	none
P1053L	-	-	-	-	-	-	-	0	none

2.2.5.2. Seven ERBB4 mutants possess a high or medium high priority score

Of the 71 ErbB4 mutants, 7 earned a medium-high or high priority mutant status (**Table 5**). Interestingly, there is a mix of those suggesting gain-of-function and loss-of-function activity.

Table 5. High and medium high priority *ERBB4* mutants.

Mutation	Priority score	Priority Rating
R106C	6	high
R711C	5	high
R992C	5	high
T422I	4	medium high
E452K	4	medium high
P759L	4	medium high
D813N	4	medium high

2.2.5.3. The high and medium-high priority mutants reside in the LBDs and tyrosine kinase domain

Once the prioritization scheme was determined, the mutants were mapped onto the ErbB4 sequence to look for potential hot spots of high and medium-high priority mutants. Half of the medium-high and high priority mutants were found in the kinase region of ErbB4 alone (**Figure 15**). The kinase region is largely responsible for signaling activity. Two of these mutations were identified as high priority candidates. The other half of the medium-high and high priority mutants were identified in the first three regions on the ligand binding domain which is important for dimerization function (**Figure 15**). No medium-high or high priority mutants were identified in the transmembrane domain, C-terminal tail, or portions of the receptor between defined domains.

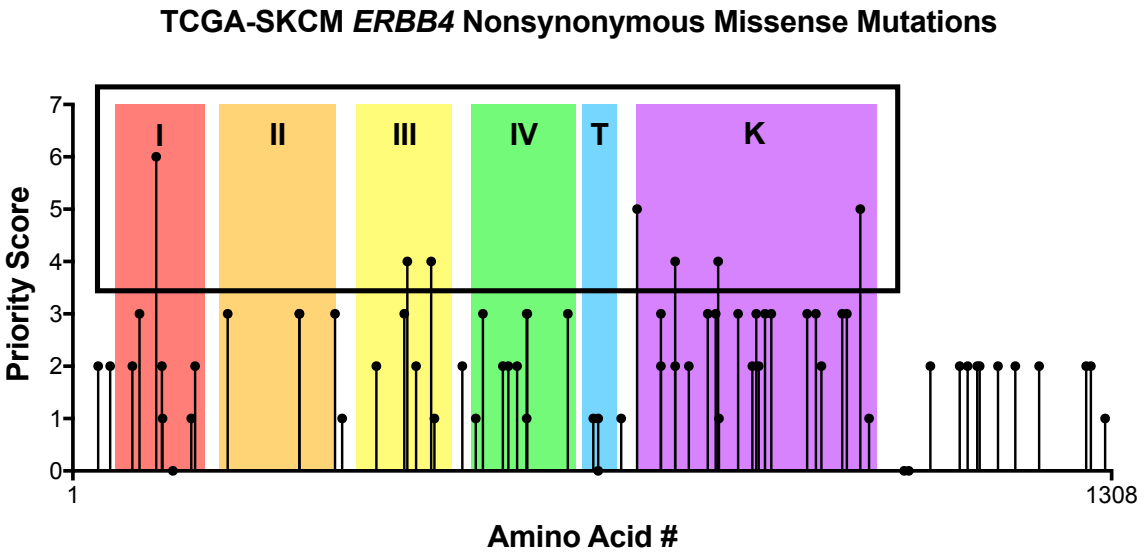

Figure 15. Lollipop plot map of prioritized ERBB4 mutants by location vs. priority score. The black box is around the medium-high and high priority candidate putative driver mutations.

2.3. Discussion

2.3.1. *ERBB4* mutations in melanoma are nonrandom and therefore are strong candidates to be melanoma drivers

Our analyses of the *ERBB4* mutations in the TCGA-SKCM dataset provide several reasons why these mutations appear to be the consequence of selection rather than random occurrence. The first of which being that the incidence of *ERBB4* missense mutations in the TCGA-SKCM dataset (20%) exceeds the incidence of *EGFR*, *ERBB2*, and *ERBB3* missense mutations. Similarly, the ratio of nonsynonymous mutations in *ERBB4* (2.9) exceeds the threshold (2.5) for candidate driver mutations [26] and exceeds the corresponding ratio in *EGFR*, *ERBB2*, and *ERBB3* (1.4, 1.2, and 1.0, respectively).

In 82 of the melanoma samples in the TCGA-SKCM dataset, a single *ERBB4* missense mutation is found. Although most (64) of these mutations are unique, 7 occur

more than once. Random assignment (100,000 simulations) of 82 missense mutations across the 1308 codons of *ERBB4* results in fewer "hot spots" for mutations than are observed ($P<0.005$, Chi-square), suggesting that melanomas select for mutations that alter ErbB4 function.

The kinase activity of ErbB4 and EGFR is stimulated by a conformational change that is stabilized by ligand binding and receptor dimerization. *ERBB4* missense mutations are more common in ErbB4 residues that are conserved in the EGFR kinase domain ($P=0.014$, Chi-square) than in ErbB4 residues that are not conserved in the EGFR kinase domain, suggesting that melanomas select for mutations that alter ErbB4 kinase activity. Additionally, *ERBB4* missense mutations are more common in ErbB4 residues that are conserved in the ligand binding domains of ErbB3. This suggests that melanomas select for mutations that alter the conformation of the extracellular domain of ErbB4.

ERBB4 missense mutations are more common in melanoma samples that possess an attribute (*NRAS*, *KRAS*, HRAS, or *NF1* driver mutations) that cause elevated RAS signaling ($P=0.001$, Chi-square). Moreover, in a very small sample, the combination of an *ERBB4* mutation with a *RAS* driver mutation is associated with shorter survival (1538 days; n=9) than the combination of wild-type *ERBB4* with a *RAS* driver mutation (2174 days; n=48). Likewise, the combination of an *ERBB4* mutation with an *NF1* driver mutation is associated with shorter survival (728 days; n=5) than the combination of wild-type *ERBB4* with an *NF1* driver mutation (1721 days; n=18). Thus, *ERBB4* mutants may not act through RAS and at least some melanomas appear to require a combination of an *ERBB4* mutation and elevated RAS signaling.

Furthermore, *ERBB4* missense mutations are less common in melanoma samples that possess an attribute (*PI3KCA* driver mutations, elevated *PI3KCA* transcription, increased *PI3KCA* copy number, *PTEN* driver mutations, reduced *PTEN* transcription, or reduced *PTEN* copy number) that results in elevated PI3K signaling (P=0.005, Chi-square). Again, this nonrandom segregation of *ERBB4* mutants suggest that melanoma selects for these mutations and that *ERBB4* missense mutants are coupled to PI3K signaling.

ERBB4 missense mutations are less common in melanoma samples that possess the *BRAF* V600E driver mutation (P=0.03, Chi-square), suggesting that *ERBB4* mutations (in combination with elevated RAS signaling) and *BRAF* V600E are independent melanoma drivers. In sum, these data suggest that at least some BRAF wild-type (WT) melanomas are dependent on the combination of an *ERBB4* mutation (or other event that causes elevated PI3K signaling) and a *RAS* or *NF1* driver mutation (which causes elevated RAS signaling). Parenthetically, these data also suggest the *BRAF* V600E mutation activates a pathway(s) in addition to the canonical RAS pathway and that activation of this additional pathway(s) is required for *BRAF* V600E to function as a melanoma driver. Thus, *ERBB4* mutations may be an important biomarker in *BRAF* WT melanomas and the combination of ErbB4/PI3K and RAS signaling may be a target for therapeutic intervention in *ERBB4* mutant/*BRAF* WT melanomas.

2.3.2. Because *ERBB4* mutations are candidates for melanoma drivers, *ERBB4* mutations in melanoma should be characterized

2.3.2.1. ErbB4-EGFR and ErbB4-ErbB2 heterodimers couple to cell proliferation.

When using BaF3 cells, ectopic expression of *ERBB4* is not sufficient for ErbB4 ligands to stimulate cell proliferation. In contrast, co-expression of either *ERBB4* and *EGFR* or *ERBB4* and *ERBB2* enables ErbB4 ligands to stimulate cell proliferation [44,45,50,51]. Likewise, inhibiting endogenous ErbB4-ErbB2 heterodimers (using siRNAs) inhibits stimulation of anchorage independent proliferation and motility by an ErbB4 ligand[45]. Analyses of synthetic *EGFR*, *ERBB2*, and *ERBB4* loss-of-function (LOF) mutants indicates that the coupling of ErbB4-EGFR or ErbB4-ErbB2 heterodimers to cell proliferation requires phosphorylation of ErbB4 Y1056 (a canonical PI3K binding site) by EGFR or ErbB2. Moreover, the coupling of ErbB4 heterodimers to cell proliferation is accompanied by AKT phosphorylation and is sensitive to PI3K inhibitors [45,48]. In melanoma samples of the TCGA-SKCM dataset, the coincidence of *ERBB4* and *EGFR* transcription is greater than the coincidence of *ERBB4* and *ERBB2* transcription, leading us to postulate that ErbB4-ErbB2 heterodimers play a greater role in melanoma genesis/progression than do ErbB4-ErbB2 heterodimers.

2.3.2.2. ErbB4 homodimers cause growth arrest and may act as tumor suppressors.

The constitutively-active ErbB4 Q646C mutant is exclusively and constitutively homodimerized [52]. This mutant inhibits clonogenic proliferation by a variety of prostate, breast, and pancreatic tumor cell lines. In the context of the *ERBB4* Q646C mutant, the K751M, Y1056F, and V673I loss-of-function mutations demonstrate that growth inhibition by ErbB4 homodimers requires ErbB4 kinase activity, phosphorylation

of ErbB4 Y1056 (PI3K binding site), and cleavage of ErbB4 and trafficking of the ErbB4 cytoplasmic domain to the nucleus [46,47,49,53,54].

2.3.2.3. ErbB4 can drive melanoma tumorigenesis through GOF and LOF mutations.

Based on these functional analyses of ErbB4 heterodimers and homodimers, *ERBB4* mutations in the TCGA-SKCM dataset may function as melanoma drivers by either (1) increasing the growth stimulatory (oncogenic) activity of ErbB4-EGFR heterodimers or (2) decreasing the growth inhibitory (tumor suppressor) activity of ErbB4 homodimers. Thus, some *ERBB4* melanoma driver mutants will exhibit a gain-of-function phenotype in the context of ErbB4-EGFR heterodimers and other *ERBB4* melanoma driver mutants will exhibit a loss-of-function phenotype in the context of ErbB4 homodimers.

Chapter 3: Development and application of high-throughput screens for the discovery of compounds that disrupt ErbB4 signaling: Candidate melanoma therapeutics

3.1. Introduction

In the last decade, the standard-of-care treatment options for patients with metastatic melanoma has significantly improved with the advent of targeted therapies and immunotherapies. In fact, recent studies with combination therapy using BRAF and MEK inhibitors and immunotherapies indicate rates of 5-year progression free survival and overall survival as high as 30-50% for metastatic melanoma patients[1-3,5,7,55]. However, many metastatic melanomas remain nonresponsive or become resistant to currently available therapeutics. Our ongoing analyses of the TCGA skin cutaneous melanoma genomic (SKCM) data set indicate that a significant fraction of melanomas likely harbor driver mutations in ERBB4 and would benefit from a therapy that disrupts ErbB4 signaling [56]. Therefore, the discovery of strategies for inhibiting ErbB4 coupling to melanoma cell proliferation is a priority.

In multiple systems, ErbB4-dependent cellular proliferation requires ErbB4 heterodimerization with EGFR or ErbB2 and ErbB4 phosphorylation by EGFR or ErbB2[44,48,50,51,57-59]. This suggests it may be possible to treat ErbB4-dependent melanomas using anti-EGFR and -ErbB2 therapies, particularly small molecule EGFR and/or ErbB2 tyrosine kinase inhibitors. Indeed, there are several FDA-approved EGFR and ErbB2 kinase inhibitors[60]. However, the responses to these therapies are often

limited by the development of resistance mechanisms[61,62]. Furthermore, targeting EGFR and ErbB2 for the treatment of ErbB4-dependent tumors could potentially affect the normal physiological roles of EGFR and ErbB2 in healthy tissue.

Consequently, we believe that compounds that function as partial agonists of ErbB4 hold great promise for the treatment of ErbB4-dependent melanomas. Our drug discovery strategy is driven by our observation that introducing the Q43L mutation into the gene that encodes the naturally-occurring ErbB4 full agonist NRG2β creates a partial agonist of ErbB4[48]; this NRG2β/Q43L mutant stimulates ErbB4 tyrosine phosphorylation, yet it inhibits agonist-induced ErbB4-dependent cell proliferation. This antagonistic activity can be overcome with an excess of wild-type NRG2β (competitive inhibition) and appears to be the effect of phosphorylation-dependent downregulation of ErbB4.

Here we have developed a screening process for identifying compounds that function as partial agonists of ErbB4. Moreover, implementation of this process has yielded several compounds that appear to selectively disrupt ErbB4 signaling, and as such are predicted to possess therapeutic potential against ErbB4-dependent tumors.

3.2. Results

3.2.1. ErbB4 tyrosine phosphorylation can be stimulated and detected via semi-automated 96-well assays

3.2.1.1. Development and validation of a 96-well sandwich ELISA for the detection of ErbB4 tyrosine phosphorylation.

Our ultimate goal is the identification of ErbB4 partial agonists that inhibit coupling of ErbB4 to cell proliferation, preferably through stimulation of phosphorylation-dependent ErbB4 turnover and degradation. Thus, the first goal of these experiments is to develop and deploy an assay for stimulation of ErbB4 tyrosine phosphorylation. The CEM/ErbB4 cell line previously validated for assaying ligand-induced ErbB4 tyrosine phosphorylation[63] was used to develop a 96-well assay for stimulation and inhibition of ErbB4 tyrosine phosphorylation. Briefly, ErbB4 tyrosine phosphorylation was assayed using a "sandwich" enzyme-linked immunosorbent assay (ELISA)[64] in which a "capture" antibody that recognizes the amino terminus of ErbB4 (R&D Systems) was bound to each well of the 96-well plate. Lysates containing total (a mixture of phosphorylated and unphosphorylated) ErbB4 were added to the wells and incubated to permit ErbB4 binding to the immobilized anti-ErbB4 antibody. Then, an anti-phosphotyrosine antibody tagged with a horseradish peroxidase (HRP) enzyme was used to detect and visualize the phosphorylated tyrosine residues of the immobilized ErbB4 molecules (R&D Systems). Oxidation of 3,3′,5,5′-tetramentylbenzidine by HRP indicates ErbB4 phosphorylation and was detected by measuring absorption at 450 nm.

Lysates generated by a previously established protocol for stimulating ErbB4 tyrosine phosphorylation in CEM/ErbB4 cells[48] were used to develop and evaluate the ELISA conditions. Briefly, the CEM/ErbB4 cells were starved for 24 hours in serum- and

factor-free base medium (RPMI) before being stimulated for seven minutes on ice with NRG2β (full agonist positive control), NRG2β/Q43L (partial agonist positive control), or NRG2β diluent (mock stimulation negative control). The cells were then lysed, and the lysates were immediately assayed for ErbB4 tyrosine phosphorylation or stored at -80 °C until assayed.

To evaluate the ELISA assay conditions, ErbB4 tyrosine phosphorylation stimulated by 10 nM NRG2β, 10 nM NRG2β/Q43L, or diluent (mock stimulation) was analyzed in eight independent ELISAs using a single batch of each of the three different lysates (**Figure 16a**). Stimulation by 10 nM NRG2β produces an average absorbance at 450 nm of 4.0 ± 0.3 AU, stimulation by 10 nM NRG2β/Q43L produces an average absorbance at 450 nm of 1.6 ± 0.2 AU, and mock stimulation produces an average absorbance at 450 nm of 0.68 ± 0.06 AU.

Using the effects of mock stimulation as the background levels of ErbB4 tyrosine phosphorylation, we determined that the average signal:noise ratio for stimulation by 10 nM NRG2β is 5.9 ± 0.7 and the average signal:noise ratio for stimulation by 10 nM NRG2β/Q43L is 2.3 ± 0.2 (**Figure 16a**).

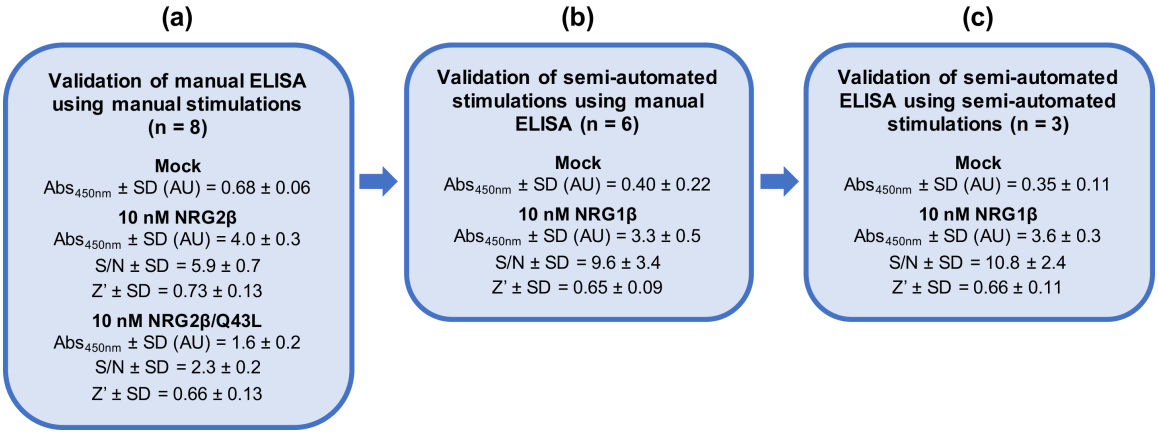

Figure 16. Validation of a semi-automated process for the stimulation and detection of ErbB4 tyrosine phosphorylation. (a) CEM/ErbB4 cells were manually stimulated with 10 nM NRG2β (full agonist positive control), 10 nM NRG2β/Q43L (partial agonist positive control), and mock (negative control). A single batch of lysate was assayed for ErbB4 tyrosine phosphorylation in eight independent trials using a manual sandwich ELISA. (b) CEM/ErbB4 cells were stimulated in six independent trials using a semi-automated protocol with 10 nM NRG1β (positive control) and mock (negative control). Each batch of lysate was assayed for ErbB4 tyrosine phosphorylation using a manual sandwich ELISA. (c) CEM/ErbB4 cells were stimulated using a semi-automated protocol with 10 nM NRG1β (positive control) and mock (negative control). A single batch of lysate was assayed for ErbB4 tyrosine phosphorylation in three independent trials using a semi-automated sandwich ELISA.

The ability of the phospho-ErbB4 ELISA to reproducibly measure ligand-induced ErbB4 tyrosine phosphorylation was formally evaluated by calculating the Z-factor (Z') values for stimulation by 10 nM NRG2β or 10 nM NRG2β/Q43L. The Z-factor is commonly used to evaluate the robustness of a high-throughput assay and is calculated using the means (μ) and standard deviations (σ) of the treatment samples (p) and untreated or negative (n) controls[65].

$$\text{Z-factor} = 1 - \frac{3(\sigma_p + \sigma_n)}{|\mu_p - \mu_n|}$$

The maximum theoretical Z-factor value is 1, whereas a Z-factor value between 0.5 and 1.0 is indicative of a robust assay. A Z-factor between 0 and 0.5 is indicative of a marginal assay[65]. Using data from eight independent ELISAs with three samples per treatment condition, stimulation with 10 nM of the ErbB4 full agonist (NRG2β) yields an average Z-factor of 0.73 and stimulation with 10 nM of the ErbB4 partial agonist (NRG2β/Q43L) yields an average Z-factor of 0.66 (**Figure 16a**). Thus, stimulation with either 10 nM NRG2β or 10 nM NRG2β/Q43L yields robust, reproducible levels of ErbB4 tyrosine phosphorylation as measured by the sandwich ELISA. Thus, this ELISA is appropriate for measuring stimulation and inhibition of ErbB4 tyrosine phosphorylation.

3.2.1.2. Validation of a semi-automated process for the stimulation of ErbB4 tyrosine phosphorylation in a 96-well format.

In order to develop an assay with the throughput needed to screen compound libraries, it was necessary to convert our standard batch method for agonist stimulation of ErbB4 tyrosine phosphorylation[48] to a semi-automated 96-well methodology. A Beckman Coulter Biomek 4000 automated liquid handling system was used to execute a semi-automated stimulation protocol that is based on our established batch protocol[48]. (The liquid-handling script for this procedure using the Biomek 4000 is available upon request.) We evaluated the robustness of this semi-automated stimulation protocol by using our validated phospho-ErbB4 ELISA assay to measure ErbB4 phosphorylation. CEM/ErbB4 cells were stimulated with 10 nM of the ErbB4 full agonist NRG1β or the NRG1β diluent (0.1% BSA in PBS) and ErbB4 tyrosine phosphorylation was assayed in wells that each contain a lysate generated from $3x10^5$ cells (**Figure 16b**). Based on six

independent trials that each utilized three wells for each experimental condition, stimulation with NRG1β (10 nM) produces an average absorbance at 450 nm of 3.3 ± 0.5 AU and mock stimulation produces an average absorbance at 450 nm of 0.40 ± 0.22 AU. Thus, the average signal:noise ratio for stimulation with NRG1β (10 nM) is 9.6 ± 3.4. It should be noted that the signal:noise ratio for semi-automated stimulation with 10 nM NRG1β is almost twice the signal:noise ratio for manual stimulation with 10 nM NRG2β (**Figure 16b**). This appears to be largely due to the decreased amount of (background) ErbB4 tyrosine phosphorylation stimulated by the diluent negative control. Furthermore, the six trials of semi-automated stimulation with 10 nM NRG1β yields an average ErbB4 tyrosine phosphorylation Z-factor (Z') score in excess of 0.6 (**Figure 16b**), which indicates that semi-automated stimulation with 10 nM NRG1β yields robust and reproducible ErbB4 tyrosine phosphorylation that is suitable for deployment in a high-throughput workflow.

3.2.1.3. Validation of a semi-automated phospho-ErbB4 sandwich ELISA in 96-well format for the detection of ErbB4 tyrosine phosphorylation.

In an attempt to make additional improvements to throughput and reproducibility, we developed and evaluated a semi-automated sandwich ELISA protocol in a 96-well format. Once again, the Biomek 4000 was used to adapt the existing phospho-ErbB4 ELISA protocol to a semi-automated workflow. (The liquid-handling script for this procedure using the Biomek 4000 is available upon request.) The ErbB4 full agonist NRG1β (10 nM) was used as the positive control for stimulation of ErbB4 tyrosine phosphorylation and the NRG1β diluent (0.1% BSA in PBS) was used as the negative

control. For comparison purposes, non-automated and semi-automated ELISAs were performed on wells that each contain a lysate prepared from $3x10^5$ cells. In three independent semi-automated ELISAs performed using a single batch of lysate (**Figure 16c**) and three wells for each experimental condition, stimulation with NRG1β (10 nM) yields an average absorbance at 450 nm of 3.6 ± 0.3 AU and stimulation with NRG1β diluent (mock) yields an average absorbance at 450 nm of 0.35 ± 0.11 AU. Based on these results, the average signal:noise ratio for stimulation with 10 nM NRG1β is 10.8 ± 2.4. Thus, the fully semi-automated process exhibits the highest S/N and the lowest noise levels of all three techniques that were used (**Figure 16**). Furthermore, assaying stimulation of ErbB4 phosphorylation (by 10 nM NRG1β) using the semi-automated ELISA yields an average Z-factor (Z') score of 0.66. Therefore, the semi-automated processes for stimulation and detection of ErbB4 tyrosine phosphorylation are suitable for use in a high throughput screening process. Given the cost of the ELISA assay reagents and other consumables, and based on three replicates per sample and three independent trials, it costs $15 to test a single concentration of a single compound for stimulation of ErbB4 tyrosine phosphorylation.

3.2.2. ErbB4-dependent cellular proliferation can be stimulated and detected via semi-automated 96-well assays

Because our ultimate goal is the identification of compounds that inhibit ErbB4-dependent cell proliferation, we sought to develop a semi-automated 96-well assay for ErbB4-dependent cell proliferation that could be deployed to identify inhibitors.

Mouse BaF3 pro-B-lymphocyte cells do not endogenously express EGFR, ErbB2, or ErbB4 and their survival and proliferation requires the exogenous growth factor interleukin-3 (IL3). However, a BaF3 cell line that expresses exogenous EGFR and ErbB4 exhibits IL3-independent proliferation upon stimulation with the ErbB4 full agonist NRG1β. This proliferation is dependent upon exogenous ErbB4 expression[51]. Therefore, the BaF3/EGFR+ErbB4 cell line[51] was used to assay ErbB4-dependent, IL3-independent cell proliferation (henceforth referred to as ErbB4-dependent proliferation).

We used an established manual 24-well assay[51] as the basis for developing a semi-automated 96-well assay for stimulation and detection of ErbB4-dependent cellular proliferation. (The liquid-handling script for this procedure using the Biomek 4000 is available upon request.) The ErbB4 full agonist NRG1β was used as the positive control. Briefly, BaF3/EGFR+ErbB4 cells were grown to saturation ($2.5x10^6$ cells/mL) and aseptically seeded at $1x10^4$ cells/well (100 μL @ $1x10^5$ cells/mL) into a sterile 96-well microplate in the absence of IL3. The cells were then treated with increasing concentrations of NRG1β in triplicate. The plate was incubated at 37 °C and 5% CO_2 for 120 hours before cell proliferation was analyzed using an MTT assay[66]. Briefly, cells were treated by directly adding 10 μL of MTT Reagent (3-(4,5-dimethylthiazol-2-yl)-2,5-diphenyltetrazolium bromide; ATCC® 30-1010K™) to the culture medium in each well and incubated in the dark for two hours at 37 °C and 5% CO_2. Then, 100 μL of Detergent Reagent (ATCC® 30-1010K™) was added to each well and the plate was incubated in the dark overnight at room temperature. MTT conversion was then determined by measuring the absorbance of each well at 570 nm. The dose response data was then analyzed using

GraphPad Prism to determine the EC_{50} and E_{max} for NRG1β. In this assay, MTT conversion is a function of viable cell number, not a function of cell metabolism (data not shown).

In four independent trials (**Figure 17a**) with three wells per treatment condition, NRG1β exhibits an average EC_{50} of 0.10 ± 0.02 nM. Furthermore, stimulation with 0.3 nM NRG1β yielded an average ErbB4-dependent cell proliferation Z-factor (Z') score of 0.80 ± 0.06. This Z-factor calculation verifies that NRB1β-induced ErbB4-dependent cellular proliferation can be reproducibly measured when BaF3/EGFR+ErbB4 cells are stimulated with 0.3 nM NRG1β. Thus, this semi-automated assay is suitable for identifying compounds that stimulate ErbB4-dependent cell proliferation. Given the cost of consumables, and based on three replicates per sample and three independent trials, it costs $2 to test a single concentration of a single compound for stimulation of ErbB4-dependent cell proliferation.

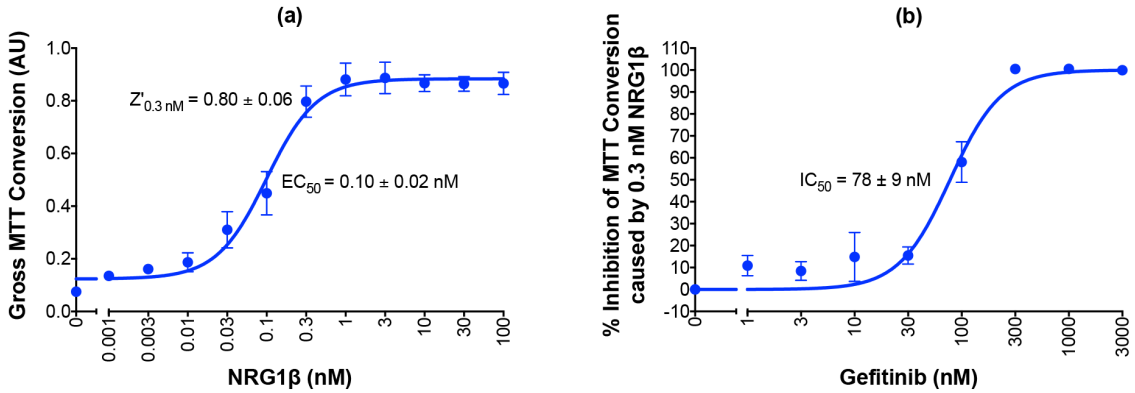

Figure 17. Validation of semi-automated processes for the stimulation of ErbB4-dependent cellular proliferation and detection of the inhibition of agonist-induced ErbB4-dependent cellular proliferation. (a) BaF3/EGFR+ErbB4 cells were stimulated with increasing concentrations of NRG1β in four independent trials using a semi-automated protocol. A semi-automated MTT assay was used to analyze cell proliferation 120 hours

post-stimulation. Curves were fit to the data using GraphPad Prism to determine the EC_{50} of NRG1β. The Z-factor for ErbB4-dependent cell proliferation stimulated by 0.3 nM NRG1β was calculated using the means and standard deviations of the positive (0.3 nM NRG1β) and negative (NRG1β-diluent) controls. (b) BaF3/EGFR+ErbB4 cells were treated with increasing concentrations of gefitinib in the presence of 0.3 nM NRG1β in four independent trials using a semi-automated protocol. A semi-automated MTT assay was used to analyze cell proliferation 120 hours post-stimulation. Curves were fit to the data using GraphPad Prism to determine the IC_{50} of gefitinib against NRG1β.

3.2.3. The inhibition of agonist-induced ErbB4-dependent cellular proliferation can be detected via semi-automated 96-well assays

In multiple model systems (including BaF3 cells), ErbB4-dependent cellular proliferation is dependent upon ErbB4 heterodimerization with EGFR or ErbB2 and ErbB4 phosphorylation by EGFR or ErbB2[44,48,50,51,57-59]. Therefore, we explored whether our semi-automated assay for ErbB4-dependent proliferation (**Figure 17a**) could be adapted to detect inhibition of ErbB4-dependent proliferation of the BaF3/EGFR+ErbB4 cell line by the EGFR tyrosine kinase inhibitor gefitinib (**Figure 17b**). (The liquid-handling script for this procedure using the Biomek 4000 is available upon request.) BaF3/EGFR+ErbB4 cells were treated with increasing concentrations of gefitinib in the presence of 0.3 nM NRG1β, a concentration of NRG1β that provides robust and highly reproducible levels of ErbB4-dependent cellular proliferation (**Figure 17a**). Four independent trials demonstrate that gefitinib completely inhibits stimulation of proliferation by 0.3 nM NRG1β and yields an IC_{50} for gefitinib of 78 ± 9 nM; a value that is comparable to previously reported IC_{50} values for gefitinib[67,68]. Furthermore, these trials demonstrated that gefitinib markedly and reproducibly inhibits the stimulation of proliferation of BaF3/EGFR+ErbB4 cells by NRG1β; the average Z-factor resulting from treatment with 100 nM gefitinib is 0.26 ± 0.45, whereas the average Z-factor resulting

from treatment with 300 nM gefitinib is 0.74 ± 0.21. These Z-factor calculations indicate that 100 nM and 300 nM gefitinib both inhibit the proliferation of BaF3/EGFR+ErbB4 cells, but that 300 nM gefitinib is more suitable for reproducibly measuring the inhibition of BaF3/EGFR+ErbB4 cell proliferation. Thus, this semi-automated proliferation assay can be used for the high-throughput identification and characterization of compounds that inhibit agonist-induced ErbB4-dependent cellular proliferation and 300 nM gefitinib can serve as a positive control for inhibition of agonist-induced ErbB4-dependent cellular proliferation.

3.2.4. Screening process for the identification of small molecule compounds that function as inhibitors of agonist-induced ErbB4-dependent cellular proliferation

3.2.4.1. Overview.

Our strategy for deploying our screens to identify compounds that may function as inhibitors of ErbB4-dependent proliferation is described in **Figure 18**. As noted elsewhere, our strategy is intended to identify ErbB4 partial agonists; such molecules stimulate ErbB4 tyrosine phosphorylation, yet fail to stimulate ErbB4-dependent cell proliferation and inhibit stimulation of ErbB4-dependent cell proliferation by an ErbB4 agonist.

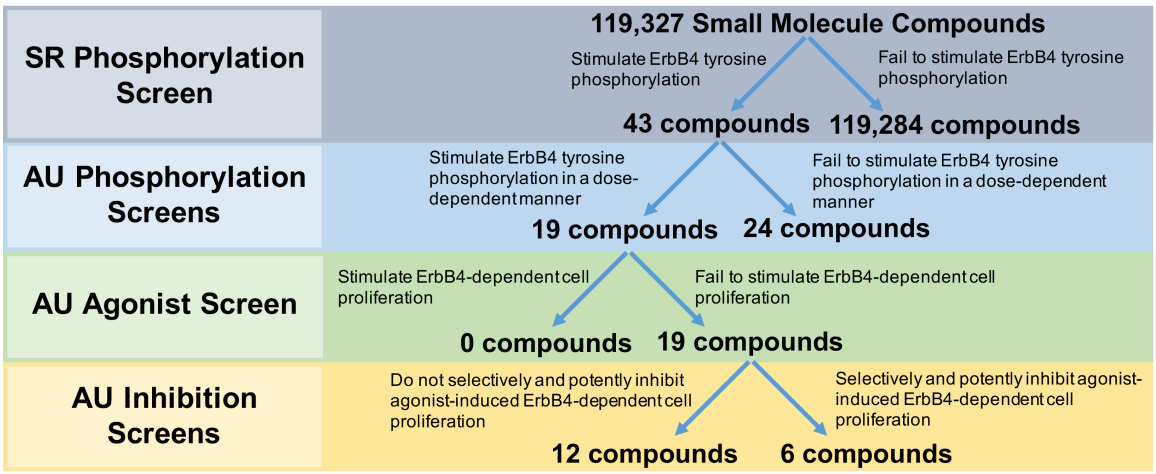

Figure 18. Deployment strategy of screening methodologies for the identification of partial agonists at the ErbB4 receptor tyrosine kinase that function as ErbB4 antagonists. Southern Research (SR) Phosphorylation Screen: SR screened a library of small molecule compounds for stimulation of ErbB4 tyrosine phosphorylation using an ultra-high throughput assay developed by DiscoverX. Auburn University (AU) Phosphorylation Screens: The 43 most promising compounds identified from the high-throughput SRI screen were then tested for concentration-dependent stimulation of ErbB4 tyrosine phosphorylation. AU Agonist Screen: The compounds that exhibited dose-dependent stimulation of ErbB4 tyrosine phosphorylation were tested to determine whether they stimulated ErbB4-dependent cellular proliferation. AU Inhibition Screens: The compounds that failed to stimulate ErbB4-dependent cellular proliferation were tested to determine whether they inhibited agonist-induced ErbB4-dependent cellular proliferation. Selectivity of these inhibitors was determined by comparing inhibition of ErbB4-dependent cellular proliferation against inhibition of Interleukin 3-dependent (IL3-dependent) cellular proliferation.

To identify ErbB4 agonists, a high throughput screen (HTS) of a structurally diverse set of 119,327 small molecule compounds selected from the compound collection maintained at Southern Research (Birmingham, Alabama) was performed using the DiscoverX PathHunter® U2OS ErbB4 Functional Assay to measure stimulation of ErbB4 tyrosine phosphorylation[26]. This assay utilizes a cell line (U2OS) that is engineered to express a recombinant ErbB4 that has been tagged with a ProLink™ (PK) epitope at the intracellular carboxyl terminus of the receptor. The cell line also expresses

a recombinant SH2 domain that is selective for binding to phosphorylated ErbB4 and has been fused to an Enzyme Acceptor (EA) epitope. Upon phosphorylation of the recombinant ErbB4-ProLink molecule, it binds the SH2-EA and the proximity of the two recombinant proteins creates an active β-galactosidase (β-gal) enzyme. β-gal activity is quantified using a chemiluminescent substrate. Using this platform, stimulation with the ErbB4 full agonist NRG1β (100nM) resulted in a two-fold increase in signal compared to negative control cells treated with vehicle. A total of 32 positive and 32 negative control wells were included in each of the 400 plates run in the HTS campaign and the signals resulted in an average Z-factor of 0.33.

Using two-fold stimulation as the threshold for compound activity, the HTS identified 132 compounds that stimulated ErbB4 tyrosine phosphorylation. Of these, 43 compounds were confirmed by exhibiting concentration-dependent activity when retested over a concentration range of 0.1 to 60 μg/ml. These 43 compounds were then subjected to the semi-automated screening processes described previously in this report, resulting in 19 compounds that inhibited ErbB4 coupling to cell proliferation, including six that appear to function as selective ErbB4 inhibitors (**Figure 18**).

3.2.4.2. Nineteen candidates stimulated ErbB4 tyrosine phosphorylation in a dose-dependent manner.

All 43 compounds that stimulate ErbB4 tyrosine phosphorylation were tested at a single concentration (10 μM) for stimulation of ErbB4 tyrosine phosphorylation using our semi-automated ELISA-based screening process (n = 3). Compounds that stimulated ErbB4 tyrosine phosphorylation in at least two of three independent trials were

subsequently tested at a range of concentrations (0 – 30 μM) in at least three independent trials to determine whether the compounds stimulated ErbB4 tyrosine phosphorylation in a concentration-dependent manner. The data obtained from testing three of the compounds that stimulated ErbB4 tyrosine phosphorylation in a concentration-dependent manner are shown in **Figure 19a-c**. The data obtained from testing one of the compounds that did not stimulate ErbB4 tyrosine phosphorylation in a concentration-dependent manner is shown in **Figure 19d**. Based on the results of these experiments, 19 compounds were judged to stimulate ErbB4 tyrosine phosphorylation and 24 were judged to be incapable of stimulating ErbB4 tyrosine phosphorylation (**Figure 18**). The EC_{50} and E_{max} were calculated for each of the 19 compounds that stimulated ErbB4 tyrosine phosphorylation (**Table 6**). The most potent compounds exhibit an EC_{50} of less than 0.3 μM and the most efficacious compounds exhibit an E_{max} in excess of 5% of the amount of ErbB4 tyrosine phosphorylation stimulated by 10 nM NRG1β.

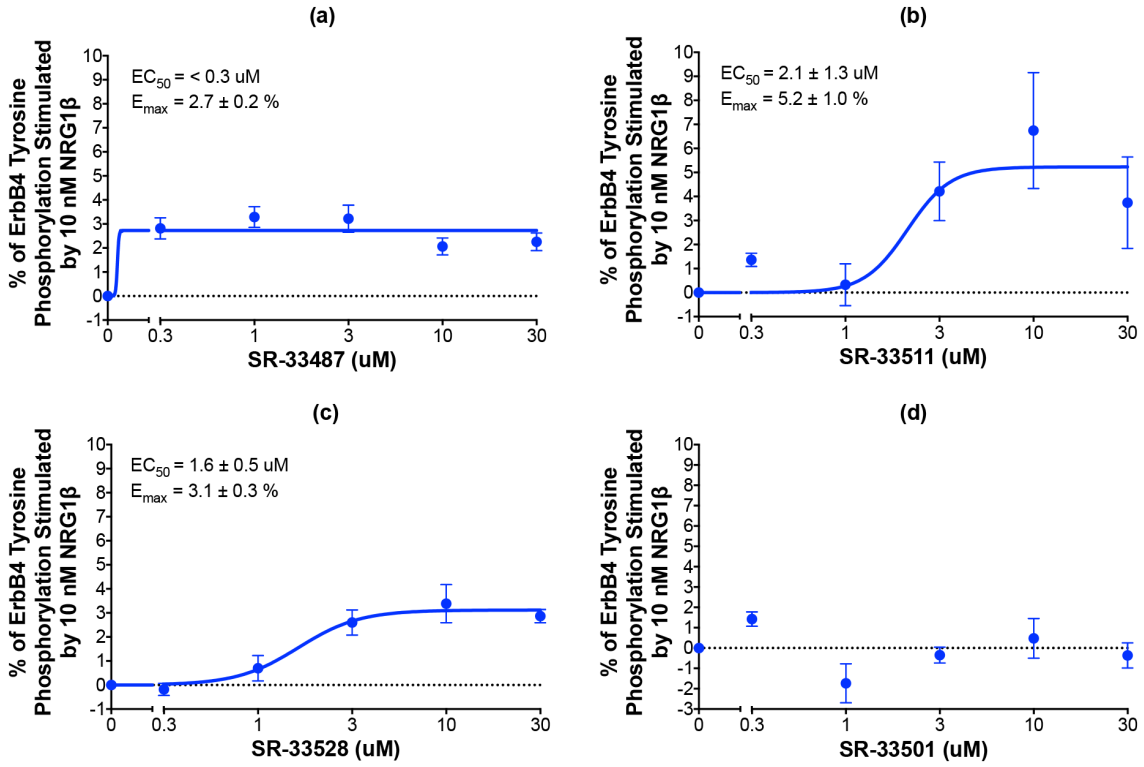

Figure 19. Representative candidates that stimulate and fail to stimulate ErbB4 tyrosine phosphorylation in a dose-dependent manner. (a-d) In at least three independent trials and using semi-automated processes, CEM/ErbB4 cells were stimulated with increasing concentrations of the candidate ErbB4 ligands. ErbB4 tyrosine phosphorylation was assayed using the semi-automated sandwich ELISA. Curves were fit to the data using GraphPad Prism to determine the EC_{50} and E_{max} values for stimulation of ErbB4 tyrosine phosphorylation by each candidate. EC_{50} and E_{max} values are also shown in **Table** 6.

Table 6. Stimulation of ErbB4 Tyrosine Phosphorylation by Candidates.

SR ID #	ErbB4 Tyrosine Phosphorylation	
	EC_{50} ± SE (μM)	**E_{max} ± SE (%)†**
SR-33486	< 0.3	5.9 ± 2.8
SR-33511	2.1 ± 1.3	5.2 ± 1.0
SR-33483	0.47 ± 0.38	4.7 ± 1.1
SR-33520	< 0.3	3.3 ± 1.0
SR-33528	1.6 ± 0.5	3.1 ± 0.3
SR-33485	< 0.3	3.0 ± 0.9
SR-33507	< 0.3	2.9 ± 0.4
SR-33491	0.68 ± 0.36	2.8 ± 0.4
SR-33519	< 0.3	2.7 ± 0.3
SR-33487	< 0.3	2.7 ± 0.2
SR-33513	< 0.3	2.4 ± 0.2
SR-33494	< 0.3	2.3 ± 0.4
SR-33493	< 0.3	2.1 ± 3.8
SR-33497	< 0.3	1.8 ± 0.5
SR-33492	4.1 ± 2.9	1.8 ± 0.2
SR-33509	0.38 ± 0.25	1.4 ± 0.3
SR-33498	1.5 ± 0.6	1.4 ± 0.4
SR-33502	< 0.3	1.4 ± 0.4
SR-33510	2.0 ± 0.8	1.2 ± 0.4

†Maximal ErbB4 tyrosine phosphorylation stimulated by candidates as a percentage of ErbB4 tyrosine phosphorylation stimulated by 10 nM NRG1β.

3.2.4.3. Nineteen candidates inhibit agonist-induced ErbB4-dependent cellular proliferation.

The 19 compounds that stimulated ErbB4 tyrosine phosphorylation in a concentration-dependent manner were then tested at a single concentration (30 μM) in three independent trials to determine whether any of the compounds also stimulated ErbB4-dependent cellular proliferation (data not shown). Using our semi-automated MTT assay, we determined that all 19 compounds fail to stimulate any ErbB4-dependent cellular proliferation (**Figure 18**). Consequently, each of these 19 compounds were then tested at a single concentration (30 μM) in combination with increasing concentrations of

an ErbB4 full agonist (NRG1β) to determine whether these compounds are capable of inhibiting agonist-induced ErbB4-dependent cellular proliferation. Based on the data shown in **Figure 17b**, gefitinib (300 nM) was used as a positive control for inhibition of agonist-induced ErbB4-dependent cellular proliferation (**Figure 20a**). At 300 nM, gefitinib reduces the E_{max} for NRG1β from 0.56 ± 0.04 AU to 0.35 ± 0.05 AU. Gefitinib shifts the EC_{50} for NRG1β from 0.08 ± 0.02 nM to 0.12 ± 0.05 nM; this very minor decrease in agonist potency is consistent with the observation that gefitinib does not directly compete with NRG1β for binding to the EGFR-ErbB4 heterodimer.

Three independent trials reveal that the candidate ErbB4 inhibitors exhibit a wide distribution of inhibitory effects on stimulation of ErbB4-dependent cellular proliferation by NRG1β (**Table 7**). Some candidates exhibit modest inhibitory efficacy, such as SR-33513 (**Table 7**). In contrast, other compounds exhibit greater efficacy, such as SR-33487, which inhibits the NRG1β E_{max} by 87% (**Figure 20b** and **Table 7**) and SR-33491, which inhibits the NRG1β E_{max} by 72% (**Figure 20c** and **Table 7**). Indeed, 30 μM of some compounds, such as SR-33507, completely inhibits cellular proliferation stimulated by NRG1β (**Figure 20d** and **Table 7**). Despite the fact that the compounds exhibit varying effects on NRG1β efficacy, none altered the potency of NRG1β in a noteworthy manner. This suggests that none of the compounds compete with NRG1β for binding to ErbB4. Nonetheless, all 19 of these compounds stimulate ErbB4 tyrosine phosphorylation in a concentration-dependent manner, fail to stimulate ErbB4-dependent cellular proliferation, and inhibit agonist-induced ErbB4-dependent cellular proliferation to some degree.

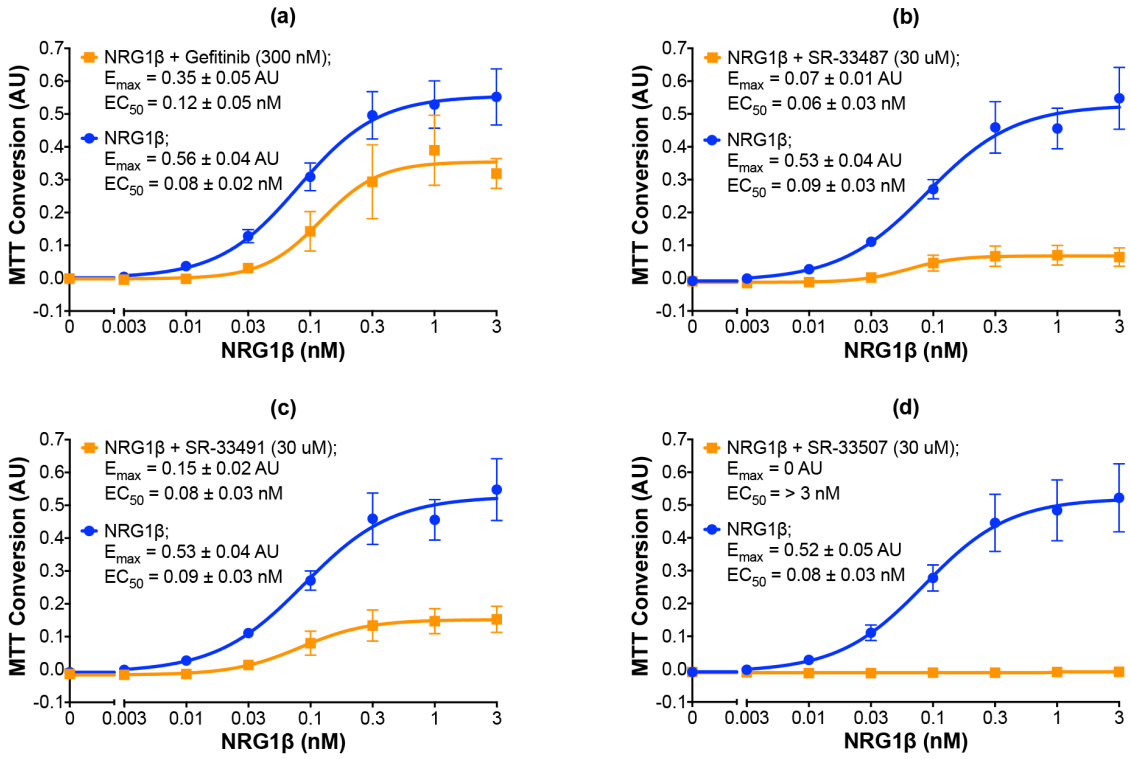

Figure 20. Representative candidates that inhibit agonist-induced ErbB4-dependent cellular proliferation. (a-d) In three independent trials and using semi-automated processes, BaF3/EGFR+ErbB4 cells were stimulated with increasing concentrations of NRG1β in the presence or absence of gefitinib at 300 nM or candidates at 30 uM. A semi-automated MTT assay was used to analyze cell proliferation at 120 hours post-stimulation. Curves were fit to the data using GraphPad Prism to determine the EC_{50} and E_{max} of NRG1β in the presence and absence of gefitinib or the candidates. EC_{50} and E_{max} values are also shown in **Table** 7.

Table 7. Effect of Candidates on Stimulation of Cell Proliferation by NRG1β.

Candidate (30 μM)	NRG1β E_{max} ± SE (AU)	NRG1β EC_{50} ± SE (nM)
None	0.54 ± 0.02	0.08 ± 0.01
Gefitinib (300 nM)	0.35 ± 0.05	0.12 ± 0.05
SR-33483	0	> 3
SR-33486	0	> 3
SR-33493	0	> 3
SR-33494	0	> 3
SR-33498	0	> 3
SR-33507	0	> 3
SR-33511	0	> 3
SR-33528	0	> 3
SR-33485	0.01 ± 0.02	0.52 ± 0.71
SR-33510	0.03 ± 0.01	0.11 ± 0.08
SR-33492	0.03 ± 0.01	0.15 ± 0.11
SR-33487	0.07 ± 0.01	0.06 ± 0.03
SR-33497	0.09 ± 0.02	0.05 ± 0.03
SR-33509	0.11 ± 0.02	0.09 ± 0.06
SR-33491	0.15 ± 0.02	0.08 ± 0.03
SR-33519	0.18 ± 0.03	0.08 ± 0.04
SR-33520	0.26 ± 0.04	0.09 ± 0.05
SR-33502	0.34 ± 0.04	0.06 ± 0.02
SR-33513	0.41 ± 0.05	0.09 ± 0.04

3.2.4.4. Six candidates appear to selectively and potently inhibit ErbB4 coupling to cell proliferation.

As noted earlier, the BaF3/EGFR+ErbB4 cells are IL3 dependent and this dependency can be rescued by stimulation of ErbB4 coupling to cell proliferation[51]. Therefore, the specificity of each of the 19 candidate ErbB4 inhibitors was tested by assaying inhibition of ErbB4-dependent and IL3-dependent cellular proliferation in parallel. Using a slightly modified version of our existing automated protocol, we tested the effects of increasing concentrations of each compound on the effects of 0.3 nM NRG1β or 0.1 nM IL3 on proliferation of the BaF3/EGFR+ErbB4 cell line. Gefitinib

completely and potently (IC_{50} of 0.13 μM) inhibits the effect of stimulation with 0.3 nM NRG1β yet fails to inhibit the effect of stimulation with 0.1 nM IL3. Therefore, gefitinib serves as the positive control for selective inhibition of ErbB4-dependent cellular proliferation (**Figure 21a**, **Table 8**).

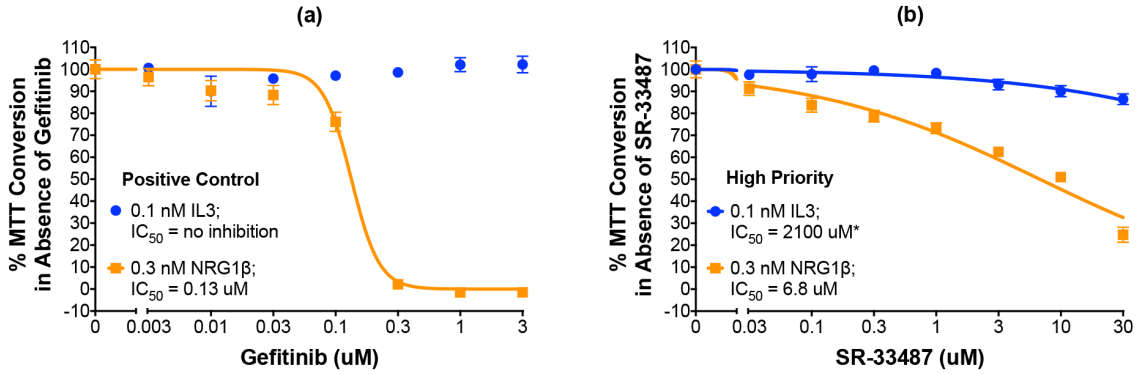

Figure 21. A high-priority small molecule compound selectively and potently inhibits ErbB4-dependent cellular proliferation. (a-b) In three independent trials and using a modified version of our semi-automated processes, BaF3/EGFR+ErbB4 cells were treated with increasing concentrations of a candidate inhibitor or gefitinib (positive control inhibitor of NRG1β-induced proliferation) in the presence of 0.1 nM IL3 or 0.3 nM NRG1β. A semi-automated MTT assay was used to analyze cellular proliferation 120 hours post-stimulation. Curves were fit to the data using GraphPad Prism to determine the IC_{50} value for each inhibitor against 0.1 nM IL3 and 0.3 nM NRG1β. IC_{50} values are also shown in **Table** 8. *Extrapolated value.

Table 8. Effect of increasing concentrations of candidate inhibitors on stimulation of cell proliferation by 0.3 nM NRG1β or 0.1 nM IL3.

Candidate	IC_{50} (μM) against 0.3 nM NRG1β	IC_{50} (μM) against 0.1 nM IL3	Priority
Gefitinib	0.13	NA	Control
SR-33528	< 0.03	< 0.03	Special Case
SR-33486	0.11	0.45	Medium
SR-33507	0.39	0.72	Low
SR-33498	2.3	4.8	Low
SR-33493	5.6	15	Low
SR-33483	6.0	28	Medium
SR-33511	6.8	13	Low
SR-33487	6.8	2100*	High
SR-33494	7.0	32*	Medium
SR-33510	11	29	Low
SR-33492	12	81*	Medium
SR-33485	13	38*	Low
SR-33491	29	NA	Medium
SR-33509	32*	NA	Low
SR-33497	47*	390*	Low
SR-33520	830*	NA	No
SR-33502	NA	NA	No
SR-33513	NA	NA	No
SR-33519	NA	NA	No

*Extrapolated value. NA = not active.

Following analysis of the data from three independent trials, the compounds were categorized based on the relative ability to selectively and potently inhibit ErbB4-dependent cellular proliferation. Six of the compounds (**Figure 21b**, **Figure 22**, **Figure 23a-e**, and **Table 8**) selectively and potently inhibit agonist-induced ErbB4-dependent cellular proliferation, twelve of the compounds do not selectively and potently inhibit agonist-induced ErbB4-dependent cellular proliferation (**Figure 22**, **Figure 24**, **Figure 25**, **Figure 26**, and **Table 8**), and one compound is considered a special case (**Figure 22**, **Figure 27** and **Table 8**).

One compound is judged to be a high priority candidate based on an IC_{50} against NRG1β-induced ErbB4-dependent cell proliferation of less than 10 μM and a selectivity for ErbB4 over IL3 (the IC_{50} value against IL3 divided by the IC_{50} value against NRG1β - $IC_{50,IL3}$:$IC_{50,NRG1\beta}$) of greater than 10. The high-priority candidate, SR-33487, inhibits the stimulation of cell proliferation by 0.3 nM NRG1β with an IC_{50} of 6.8 μM and is predicted to inhibit IL3-dependent cellular proliferation with an IC_{50} of 2100 μM (**Figure 21b**, **Figure 22** and **Table 8**). Thus, SR-33487 is a much more potent inhibitor of ErbB4-dependent cell proliferation than of IL3-dependent cell proliferation.

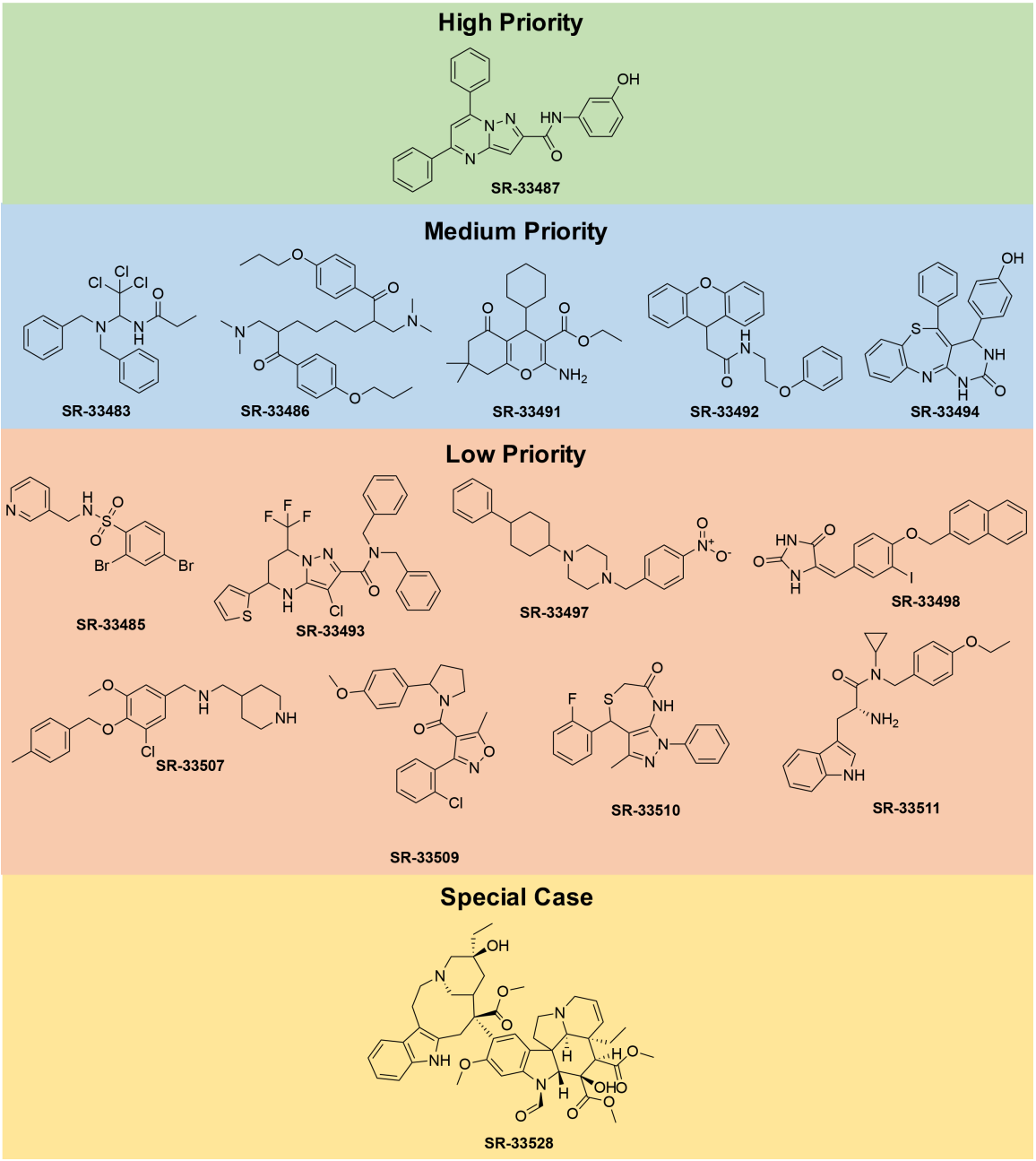

Figure 22. Chemical structures of high priority, medium priority, low priority, and special case compounds.

The remaining five compounds that selectively and potently inhibit ErbB4-dependent cell proliferation are considered medium priority candidates (**Figure 22** and **Figure 23a-e**). Medium priority candidates exhibit an IC_{50} of less than 30 μM against NRG1β-induced ErbB4-dependent cell proliferation AND a selectivity for ErbB4 over IL3 of at least 3. For example, SR-33486 inhibits the stimulation of cell proliferation by 0.3 nM NRG1β with an IC_{50} of 0.11 uM and inhibits IL3-dependent cellular proliferation with an IC_{50} of 0.45 μM (**Figure 23a** and **Table 8**). Thus, even though SR-33486 is a more potent inhibitor of ErbB4-dependent cell proliferation than is the high priority candidate (SR-33487), SR-33486 is much less selective for ErbB4 than is SR-33487.

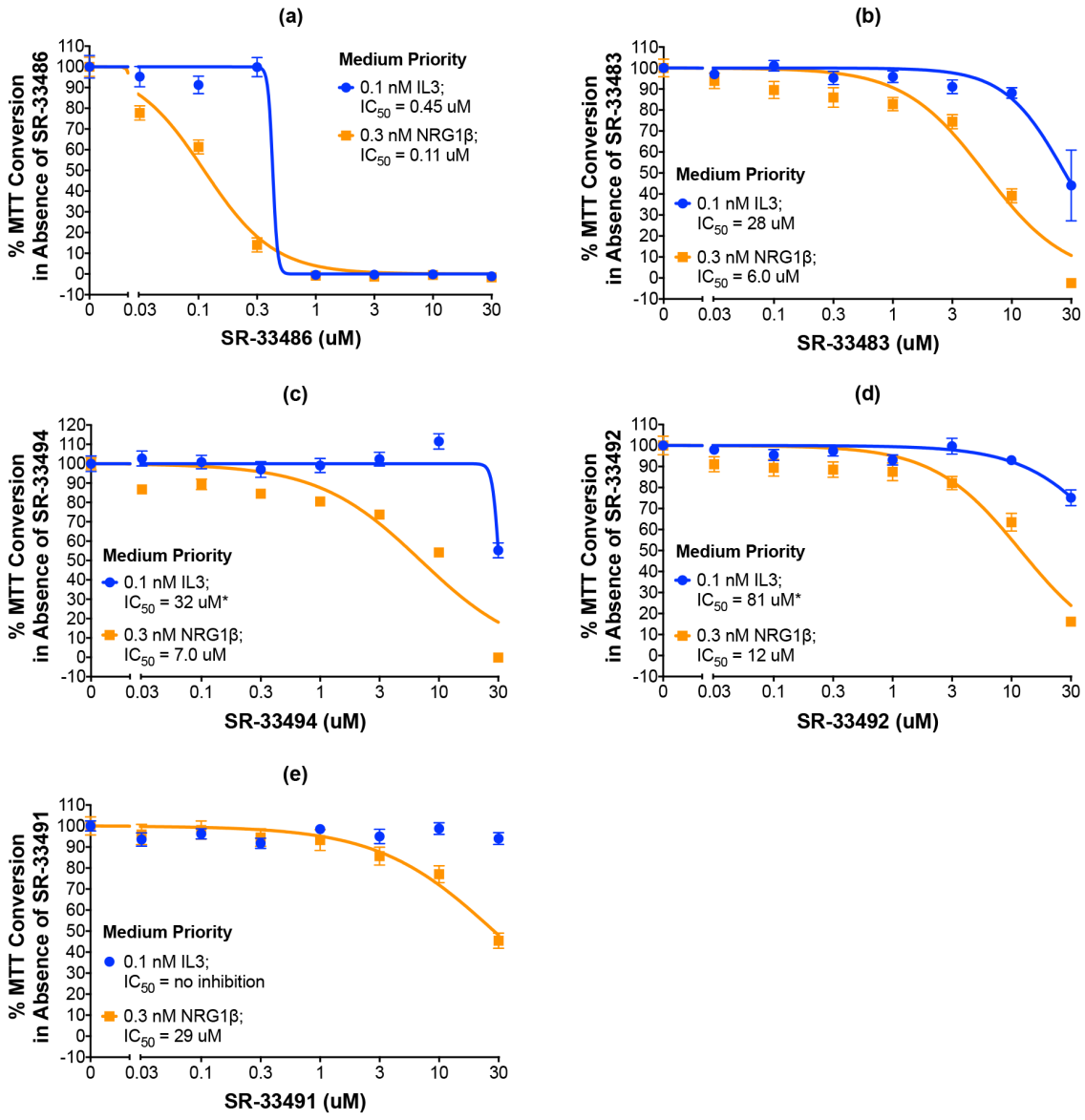

Figure 23. Five compounds are potent and selective inhibitors of ErbB4-dependent cellular proliferation. (a-e) In three independent trials and using a modified version of our semi-automated processes, BaF3/EGFR+ErbB4 cells were treated with increasing concentrations of each candidate inhibitor in the presence of 0.1 nM IL3 or 0.3 nM NRG1β. A semi-automated MTT assay was used to analyze cellular proliferation 120 hours post-stimulation. Curves were fit to the data using GraphPad Prism to determine the IC_{50} value for each candidate against 0.1 nM IL3 and 0.3 nM NRG1β. IC_{50} values are also shown in **Table** 8.

Eight compounds are judged to be low priority candidates (**Figure 22**, **Figure 24**, and **Figure 25**). Low priority candidates exhibit an IC_{50} of less than 30 μM against NRG1β-induced ErbB4-dependent cell proliferation OR a selectivity for ErbB4 over IL3 of at least 3. For example, SR-33507 inhibits the stimulation of cell proliferation by 0.3 nM NRG1β with an IC_{50} of 0.39 μM and inhibits IL3-dependent cellular proliferation with an IC_{50} of 0.72 μM (**Figure 24a** and **Table 8**). Also, SR-33509 inhibits the stimulation of cell proliferation by 0.3 nM NRG1β with an IC_{50} of 32 μM and fails to inhibit IL3-dependent cellular proliferation (**Figure 25c** and **Table 8**).

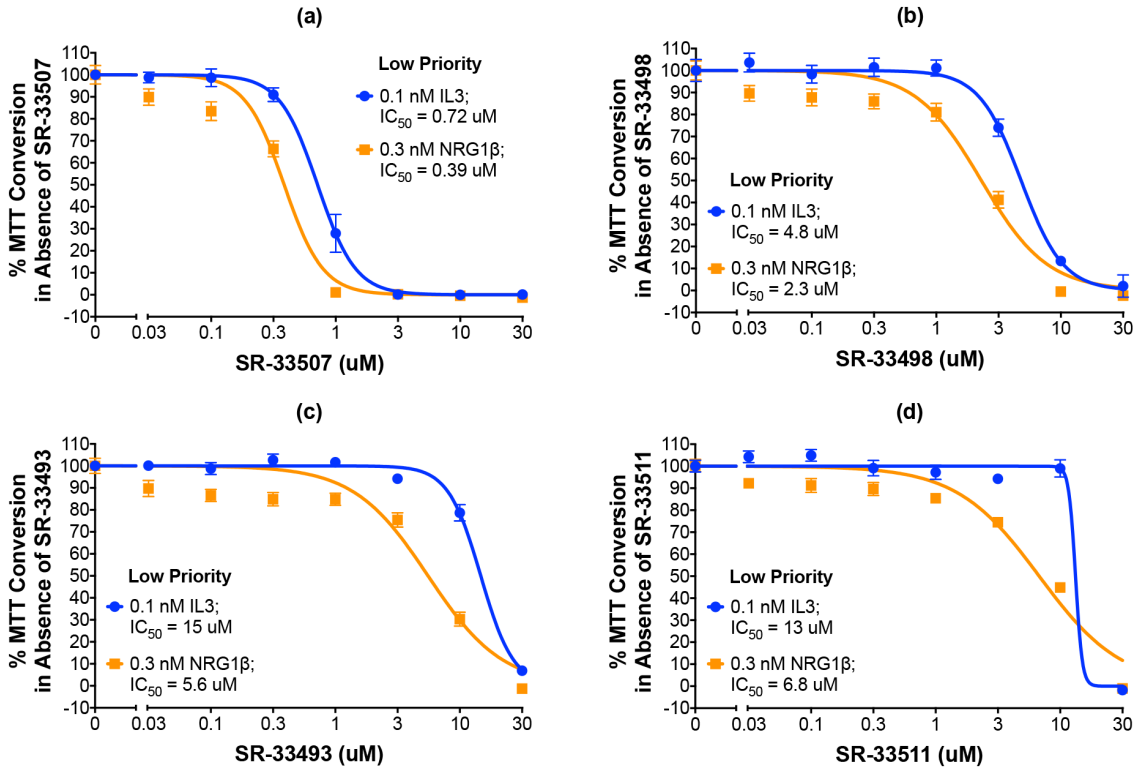

Figure 24. Four candidates do not selectively and potently inhibit ErbB4-dependent cellular proliferation. (a-d) In three independent trials and using a modified version of our semi-automated processes, BaF3/EGFR+ErbB4 cells were treated with increasing concentrations of each candidate inhibitor in the presence of 0.1 nM IL3 or 0.3 nM NRG1β. A semi-automated MTT assay was used to analyze cellular proliferation 120 hours post-stimulation. Curves were fit to the data using GraphPad Prism to determine the IC_{50} value for each candidate against 0.1 nM IL3 and 0.3 nM NRG1β. IC_{50} values are also shown in **Table** 8.

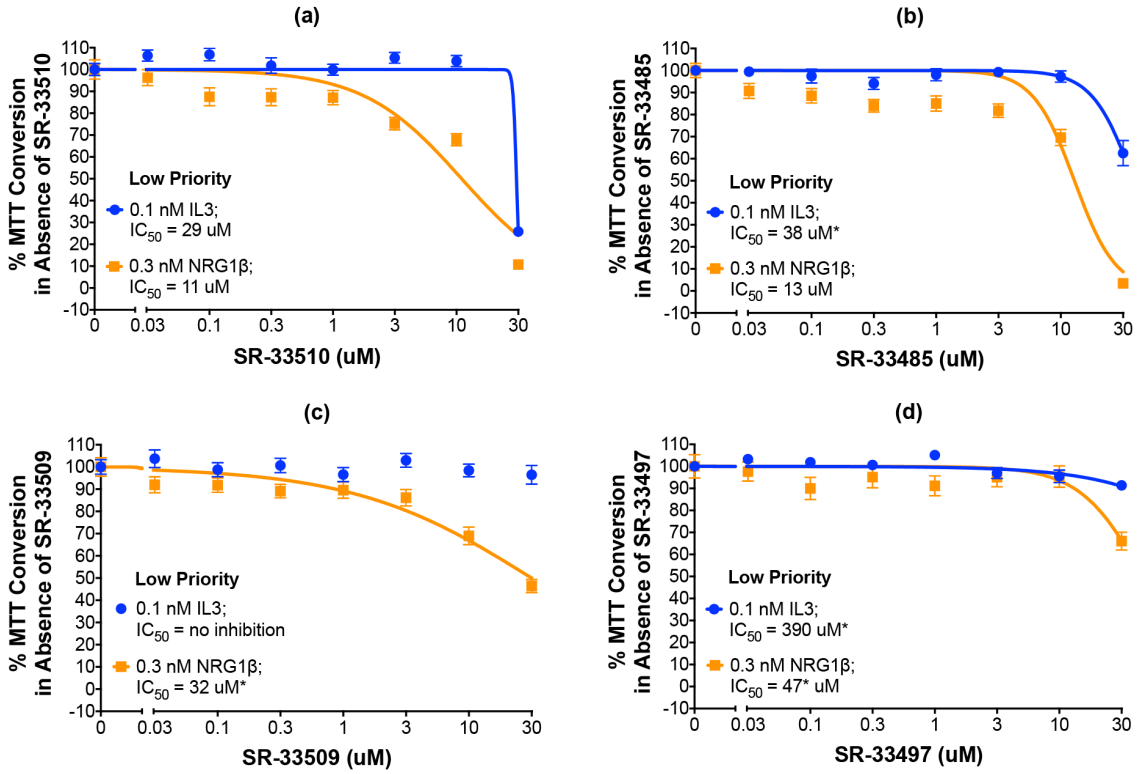

Figure 25. Four candidates do not selectively and potently inhibit ErbB4-dependent cellular proliferation. (a-d) In three independent trials and using a modified version of our semi-automated processes, BaF3/EGFR+ErbB4 cells were treated with increasing concentrations of each candidate inhibitor in the presence of 0.1 nM IL3 or 0.3 nM NRG1β. A semi-automated MTT assay was used to analyze cellular proliferation 120 hours post-stimulation. Curves were fit to the data using GraphPad Prism to determine the IC_{50} value for each candidate against 0.1 nM IL3 and 0.3 nM NRG1β. IC_{50} values are also shown in **Table** 8.

Our assays identified four compounds that do not selectively nor potently inhibit agonist-induced ErbB4-dependent cell proliferation and therefore possess no priority for further development (**Figure 22**, **Figure 26** and **Table 8**). In other words, these molecules exhibit an IC_{50} of GREATER than 30 μM against NRG1β-induced ErbB4-dependent cell proliferation AND a selectivity for ErbB4 over IL3 of LESS than 3.

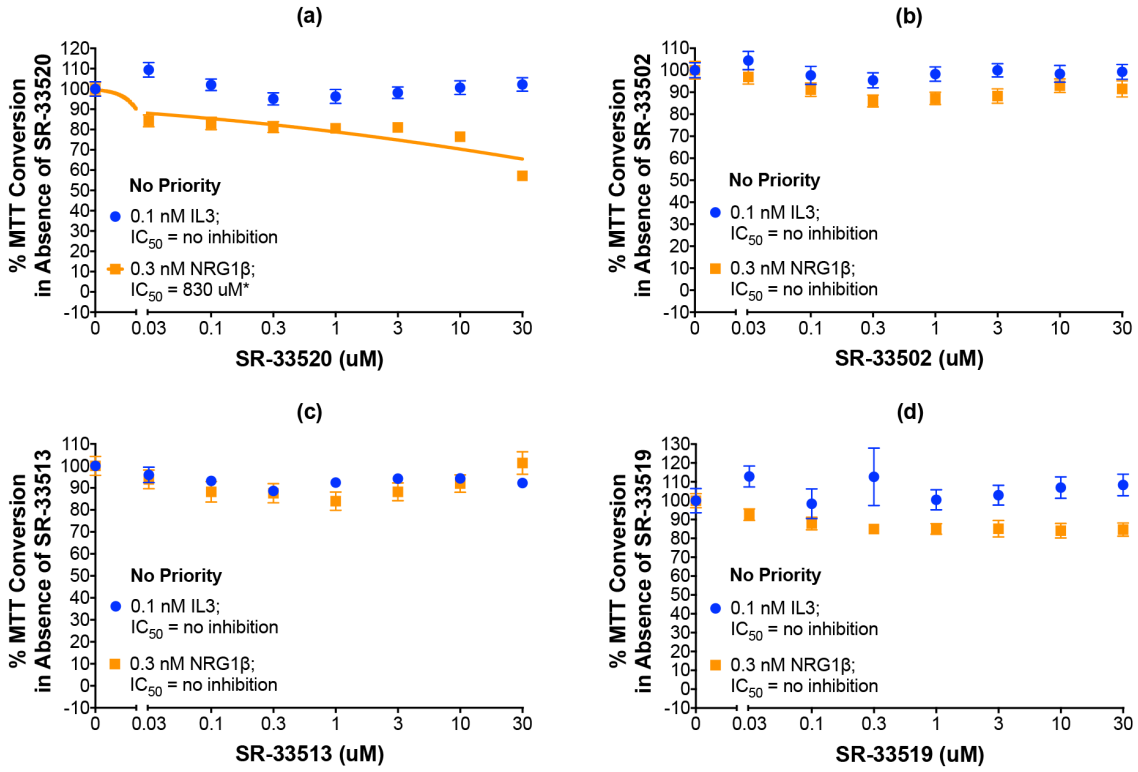

Figure 26. Four candidates are no longer under consideration. (a-d) In three independent trials and using a modified version of our semi-automated processes, BaF3/EGFR+ErbB4 cells were treated with increasing concentrations of each candidate inhibitor in the presence of 0.1 nM IL3 or 0.3 nM NRG1β. A semi-automated MTT assay was used to analyze cellular proliferation 120 hours post-stimulation. Curves were fit to the data using GraphPad Prism to determine the IC_{50} value for each candidate against 0.1 nM IL3 and 0.3 nM NRG1β. IC_{50} values are also shown in **Table** 8.

3.2.4.5. "Special case" molecule SR-33528 is not a selective inhibitor of ErbB4.

One molecule, SR-33528, is considered a special case as our initial analyses (**Figure 27a**; **Table 8**) indicate that it potently inhibits stimulation of cell proliferation by 0.3 nM NRG1β (IC_{50} of less than 30 nM) and by 0.1 nM IL3 (IC_{50} of less than 30 nM). Since this potent inhibition of ErbB4-dependent and IL3-dependent proliferation made it impossible to judge the selectivity of this candidate for inhibition of ErbB4-dependent cell proliferation, SR-33528 was evaluated at a lower concentration range (**Figure 27b**).

These data reveal that SR-33528 potently inhibits ErbB4-dependent cell proliferation (IC_{50} = 1.05 nM) and IL3-dependent cell proliferation (IC_{50} = 2.51 nM). This minimal specificity for ErbB4 over IL3 indicates that this molecule may not be a prime candidate for further development as an ErbB4 inhibitor.

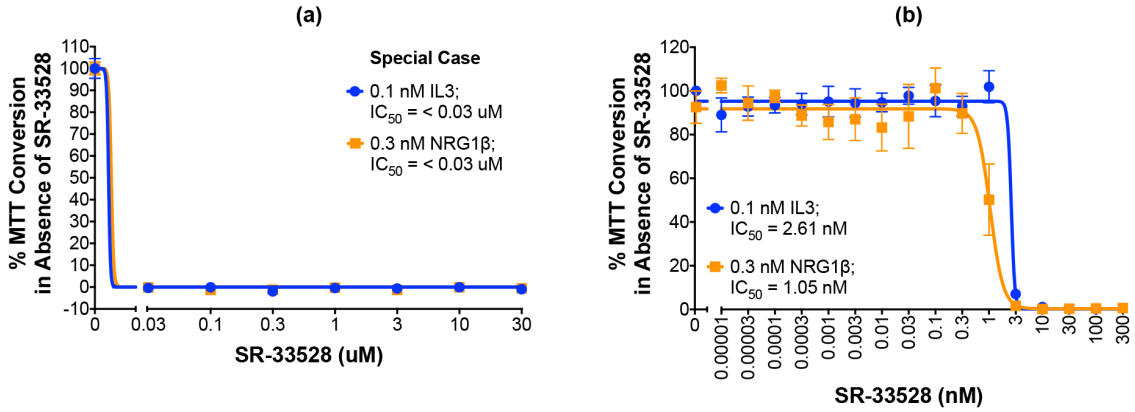

Figure 27. "Special case" molecule SR-33528 is not a selective ErbB4 inhibitor. (a-b) In three independent trials and using a modified version of our semi-automated processes, BaF3/EGFR+ErbB4 cells were treated with increasing concentrations of each candidate inhibitor in the presence of 0.1 nM IL3 or 0.3 nM NRG1β. A semi-automated MTT assay was used to analyze cellular proliferation 120 hours post-stimulation. Curves were fit to the data using GraphPad Prism to determine the IC_{50} value for each candidate against 0.1 nM IL3 and 0.3 nM NRG1β.

Due to the similarity in SR-33528 potency against ErbB4- and IL3-dependent proliferation, we postulated that SR-33528 targets a convergence point downstream of ErbB4 and the IL3 receptor (**Figure 28**). Two such candidates are the PI3K/AKT signaling pathway and the Ras/Raf/MEK/ERK signaling pathway. However, SR-33528 fails to inhibit AKT phosphorylation or ERK phosphorylation (data not shown). In light of these results, it is clear that SR-33528 does not act upstream of either AKT or ERK.

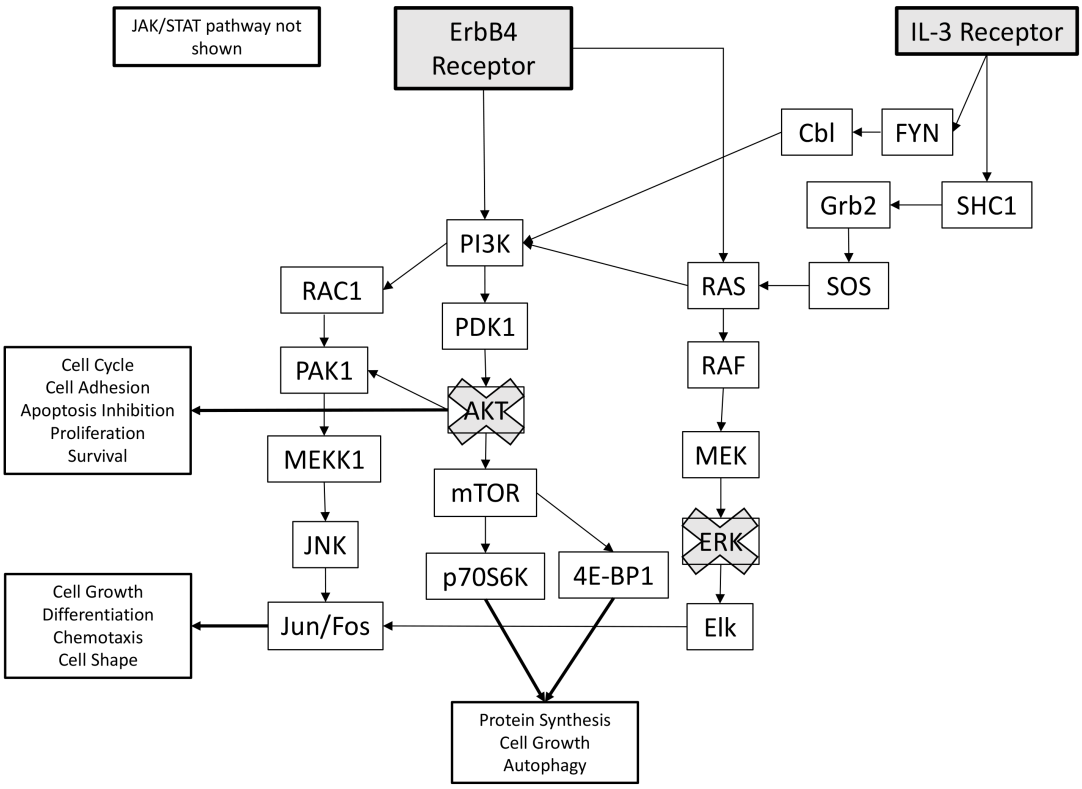

Figure 28. ErbB4 and IL3 receptor signaling pathways.

In an attempt to identify the target for SR-33528, we performed an *in silico* search for molecules whose structure is similar to SR-33528. SR-33528 is structurally very similar to vinca alkaloids, particularly the FDA-approved anticancer agent vincristine (**Figure 29**)[69]. This similarity suggests that SR-33528, like vincristine, non-specifically inhibits cell proliferation by preventing tubulin polymerization into microtubules just prior to cell division. This mechanism of action is consistent with our observation that SR-33528 inhibits ErbB4- and IL3-dependent proliferation with roughly equivalent potency.

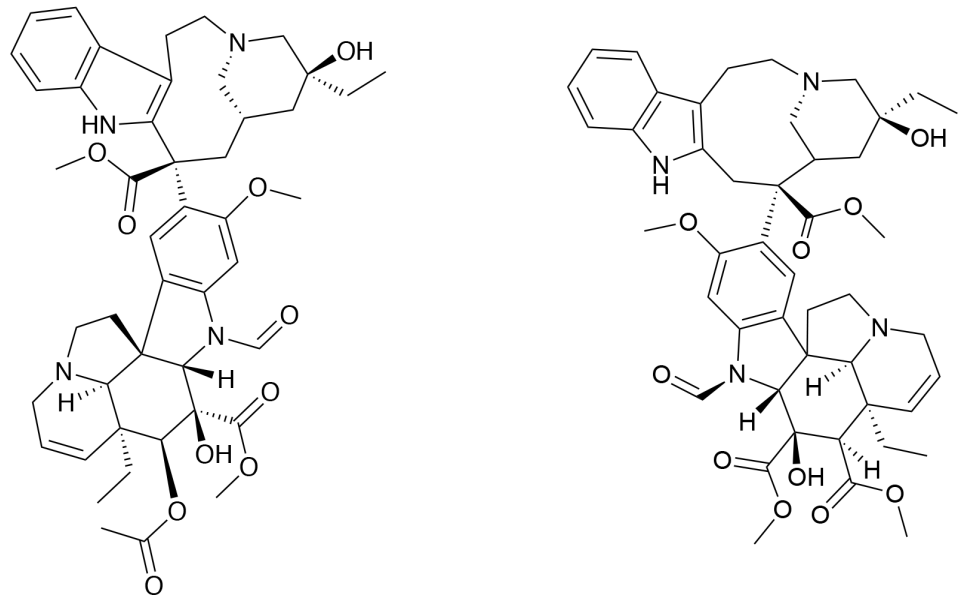

Figure 29. Chemical structures of vincristine and SR-33528.

3.3. Discussion

Due to the high mortality rate of metastatic melanoma patients, there is a critical need for the identification of additional melanoma drivers that contribute to the disease state and the discovery of treatment strategies that target these newly identified drivers. In the largest publicly available melanoma genome dataset (TCGA-SKCM), 14% of the melanomas harbor a nonsynonymous missense mutation in the gene that encodes the ErbB4 receptor tyrosine kinase (RTK)[15]. Previous analyses of the TCGA skin cutaneous melanoma genomic (SKCM) data set[56], suggests that a significant fraction of melanomas likely harbor driver mutations in *ERBB4* and would benefit from a therapy that disrupts ErbB4 signaling. Therefore, the discovery of strategies for inhibiting ErbB4 coupling to melanoma cell proliferation has valid clinical potential.

The drug discovery strategy described in this work is driven by our observation that the Q43L mutant of the naturally-occurring ErbB4 full agonist NRG2β functions as a partial agonist of ErbB4[48]. NRG2β/Q43L stimulates ErbB4 tyrosine phosphorylation, yet it fails to stimulate ErbB4-dependent cell proliferation and inhibits agonist-induced ErbB4-dependent cell proliferation, in part by causing phosphorylation-dependent downregulation of ErbB4. Therefore, our strategy is focused on identifying compounds that function as partial agonists/antagonists of ErbB4 and cause ErbB4 downregulation, as such compounds are predicted to possess therapeutic potential against ErbB4-dependent melanomas.

A high throughput screen identified 43 compounds that stimulate ErbB4 phosphorylation, as measured using the DiscoverX PathHunter® technology. Three semi-automated assays were developed and employed to identify which of these 43 compounds function as ErbB4 partial agonists/antagonists. The first assay was used to confirm which compounds stimulate ErbB4 tyrosine phosphorylation with high sensitivity and reproducibility (Z'>0.5). The second assay was used to identify compounds that stimulate ErbB4-dependent cell proliferation with high sensitivity and reproducibility (Z'>0.5). Finally, the third assay measured the effect of compounds to antagonize agonist stimulation of ErbB4-dependent cell proliferation (Z'>0.5). When applied to the 43 HTS hits, these three assays identified 19 compounds that stimulated ErbB4 tyrosine phosphorylation yet failed to stimulate ErbB4-dependent cell proliferation.

While the most efficacious compounds stimulated less than 10% of the phosphorylation stimulated by 10 nM NRG1β, each of these compounds remains a potential partial agonist of ErbB4. Previously, it has been shown that ErbB4 contains

numerous cytoplasmic tyrosine residues that become phosphorylated upon stimulation with an ErbB4 agonist[70]. However, phosphorylation of a single cytoplasmic tyrosine residue of ErbB4 is sufficient for coupling to a biological response[53]. Similarly, ErbB4 agonists stimulate ErbB4 coupling to biological responses at agonist concentrations that fail to stimulate detectable ErbB4 tyrosine phosphorylation. As seen in **Figure 17a**, 0.1 nM NRG1β is capable of stimulating a detectable amount of ErbB4-dependent cellular proliferation, but at least 1 nM NRG1β is required to stimulate a detectable amount of ErbB4 tyrosine phosphorylation (data not shown). Therefore, it remains possible that some of the inhibitors of ErbB4-dependent cell proliferation function as partial agonists at ErbB4.

Using a modified version of the tertiary screen, we tested whether any of the 19 compounds that stimulated ErbB4 tyrosine phosphorylation and failed to stimulate ErbB4 coupling to cell proliferation also selectively inhibited ErbB4-dependent proliferation. As a result, six compounds (SR-33487, SR-33486, SR-33483, SR-33494, SR-33492, SR-33491) were identified that appear to selectively and potently inhibit ErbB4-dependent cell proliferation (**Figure 21b**, **Figure 23a-e**, **Table 8**).

Much work beyond the scope what is described here is needed to advance the six compounds that appear to selectively and potently inhibit ErbB4-dependent cell proliferation. The mechanism(s) of action remains to be identified. Should these compounds function as *bona fide* direct inhibitors of ErbB4, traditional QSAR approaches will need to be deployed to improve the potency (and if necessary, selectivity) of these compounds. Of course, challenges of drug delivery, bioavailability, pharmacokinetics, and pharmacodynamics will need to be overcome. Nonetheless, these

future efforts and challenges do not discount the importance of this work in establishing plausible, scalable approaches for identifying ErbB4 inhibitors.

3.4. Materials and Methods

3.4.1. Cell lines, cell culture, recombinant NRGs, and inhibitors

The CEM/ErbB4 cells[63] were a gift from Dr. Gregory D. Plowman (Eli Lilly and Company, New York, New York, USA) through Dr. David F. Stern (Yale University, New Haven, Connecticut, USA). The BaF3/EGFR+ErbB4 cells have been described previously[51]. The U2OS cells (Catalog number 93-0465U3) were purchased from DiscoverX. Cell culture media and supplements were obtained from HyClone/Thermo Scientific, Gemini Bio-Products, DiscoverX, and Corning. All cell lines were maintained according to published procedures. Recombinant NRG1β was obtained from PeproTech, and NRG2β isoforms and mutants have been described previously[57,59,71]. We have also previously described the procedures for expressing, purifying, and quantifying recombinant proteins[71]. The EGFR tyrosine kinase inhibitor gefitinib was acquired from Santa Cruz Biotechnology. The small-molecule compounds were provided by Southern Research (Birmingham, Alabama, USA).

3.4.2. DiscoverX PathHunter® U2OS ErbB4 Functional Assay

U2OS cells were cultured and the assay was performed according to the DiscoverX protocol[26]. On assay day one, 20 µL cells were added to each well of the plates at a concentration of 400,000 cells/mL for the final count of 8000 cells/well. The assay plates were incubated overnight at 37 °C and 5% CO_2 in a humidified atmosphere.

On day two, compounds were diluted in assay medium (DiscoverX catalog number 93-0563R16B) to prepare a 5x concentrated dosing solution (50 µg/mL) and added to equilibrated assay plates in 5 µL (1/5 final well volume) to give a final compound concentration of 10 µg/mL and a final DMSO concentration of 0.2%. Assay medium alone (at 0.2% DMSO) served as the negative control and 100 nM NRG1β (at 0.2% DMSO) as the positive control. Drugging times were recorded, and plates were incubated at room temperature for 3 hours. Twelve (12) µL of detection reagent was added to the assay plates. Following 1h room-temperature incubation, ultrasensitive luminescence was read on a PerkinElmer EnVision plate reader.

3.4.3. Manual ligand stimulation and detection of ErbB4 tyrosine phosphorylation in CEM/ErbB4 cells

Ligand-induced ErbB4 tyrosine phosphorylation was stimulated using a published protocol[48]. Briefly, the CEM/ErbB4 cells were starved for 24 hours in serum- and factor-free base medium (RPMI) before being stimulated for 7 minutes on ice with an ErbB4 ligand (NRG1β, NRG2β, or NRG2β/Q43L) or candidate small molecule ErbB4 partial agonists. The cells were then lysed using a published protocol[48], and the lysates were immediately assayed for ErbB4 tyrosine phosphorylation or stored at -80 °C until assayed.

ErbB4 tyrosine phosphorylation was analyzed using a 96-well “sandwich” enzyme-linked immunosorbent assay (ELISA). First, each well in a 96-well flat-bottom plate (ELISA plate) was coated with a capture antibody (R&D Systems anti-ErbB4) that recognizes the amino terminus of ErbB4. Nonspecific binding sites were then treated with a blocking buffer (1% BSA in PBS). Lysate samples containing ErbB4 were then

added to the wells and incubated to permit ErbB4 binding to the immobilized anti-ErbB4 antibody. Then, an anti-phosphotyrosine antibody tagged with a horseradish peroxidase (HRP) enzyme (R&D Systems) was used to detect and visualize the phosphorylated tyrosine residues of the immobilized ErbB4 molecules. Oxidation of 3,3′,5,5′-tetramentylbenzidine by HRP (stopped using sulfuric acid) is indicative of ErbB4 tyrosine phosphorylation and was detected by measuring absorption at 450 nm.

3.4.4. Automated ligand stimulation and detection of ErbB4 tyrosine phosphorylation in CEM/ErbB4 cells

A Beckman Coulter Biomek 4000 automated liquid handling system was used to convert our standard, batch method for agonist stimulation of ErbB4 tyrosine phosphorylation [48] to a semi-automated 96-well methodology. (The liquid-handling script for this procedure using the Biomek 4000 is available upon request.) Briefly, the CEM/ErbB4 cells were starved for 24 hours in serum- and factor-free base medium (RPMI) before being stimulated in triplicate in 96-well conical-bottom plates (stimulation plates) for 7 minutes at 4 °C and shaking with an ErbB4 ligand (NRG1β) or candidate small molecule ErbB4 partial agonists. After stimulation, lysis buffer was added to each well and incubated for 20 minutes at 4 °C with shaking. Following incubation, the plates were centrifuged at 3200 RCF for 20 minutes at 4 °C. The supernatants (lysate samples) were then immediately transferred to an ELISA plate and assayed for ErbB4 tyrosine phosphorylation or transfer to a storage plate and stored at -80 °C until assayed.

Once again, a Biomek 4000 was used to convert the existing phospho-ErbB4 ELISA protocol to a semi-automated 96-well format. (The liquid-handling script for this procedure using the Biomek 4000 is available upon request.) Lysate samples were

transferred from the 96-well stimulation plates to the 96-well ELISA plates that were precoated with the previously mentioned capture antibody. The phospho-ErbB4 ELISA was then completed as described previously using the Biomek 4000.

3.4.5. Automated ligand stimulation and detection of ErbB4 coupling to IL-3 independence

We used an established manual 24-well assay[51] as the basis for developing a semi-automated 96-well assay for stimulation and detection of ErbB4-dependent cellular proliferation. (The liquid-handling script for this procedure using the Biomek 4000 is available upon request.) Briefly, BaF3/EGFR+ErbB4 cells were grown to saturation ($2.5x10^6$ cells/mL) and aseptically seeded at $1x10^4$ cells/well (100 uL @ $1x10^5$ cells/mL) into a sterile 96-well microplate in the absence of IL3. The cells were then treated with an ErbB4 ligand (NRG1β) in triplicate. In studies of the inhibition of ErbB4-dependent cellular proliferation, the cells were treated with an ErbB4 ligand (NRG1β) in triplicate in the presence or absence of the EGFR tyrosine kinase inhibitor gefitinib or candidate small molecule inhibitors. The plate was incubated at 37 °C and 5% CO_2 for 120 hours before cell proliferation was analyzed using an MTT assay[66]. Briefly, cells were treated by directly adding 10 uL of MTT Reagent (3-(4,5-dimethylthiazol-2-yl)-2,5-diphenyltetrazolium bromide; ATCC® 30-1010K™) to the culture medium in each well and incubated in the dark for 2 hours at 37 °C and 5% CO2. Then, 100 uL of Detergent Reagent (ATCC® 30-1010K™) was added to each well and the plate was incubated in the dark overnight at room temperature. MTT conversion was then determined by measuring the absorbance of each well at 570 nm. Dose response data was then analyzed using GraphPad Prism to determine the EC_{50} and E_{max} for NRG1β or the IC50 and Imax

for inhibitors in the presence of NRG1β. In this assay, MTT conversion is a function of differences in viable cell number, not a function of differences in cell metabolism (data not shown).

3.4.6. Analyses of SR-33528 function

3.4.6.1. Treatment with SR-33528, NRG1β, and IL3

Analyses of SR-33528 function were performed using strategies similar to those used to study the antagonistic ErbB4 ligand NRG2β/Q43L[48]. Briefly, BaF3/EGFR+ErbB4 cells were grown to saturation density in growth medium at 37°C and 5% CO_2. Cells were then starved in basal medium at half the original volume for 24 hours. Cells were re-suspended in PBS at a density of $1.5x10^7$ cells/mL, aliquoted such that each sample contained 1 mg of protein and treated for 2 hours at 37°C with 0, 0.3, 1.0, and 3.0 μM SR-33528 at a final DMSO concentration of 0.3%.

Samples used to study ErbB4 phosphorylation were chilled on ice for 30 minutes. These cells were stimulated by 30 nM NRG1β or 3 nM IL 3 for 7 minutes at 4°C (on ice). Samples used to study events downstream of ErbB4 or the IL3 receptor were incubated in a 37°C water bath. These cells were stimulated by 30 nM NRG1β or 3 nM IL 3 for 2 minutes at 37°C

After stimulation, cells were collected by centrifugation at ~10,000 g for one minute and resuspended at a concentration of $1.5x10^7$ cells/mL in an EBC isotonic lysis buffer consisting of 50 mM Tris (pH 7.6), 120 mM NaCl, 0.5% Igepal CA-630, 1% Aprotinin, and 1 mM Na_3VO_4. Cells were incubated in lysis buffer for 20 minutes on ice. Nuclei and debris were collected by centrifugation at ~10,000 g for one minute. The

supernatant (cytoplasmic and plasma membrane lysate) was recovered and either immediately used or aliquoted and stored at -80°C. The lysis of $1.5x10^7$ cells yields 1 mg of protein.

3.4.6.2. ErbB4 immunoprecipitation

Analyses were performed using lysates prepared for the purpose of evaluating ErbB4 phosphorylation. For each immunoprecipitation, 35 uL of a 50% slurry of Protein A Sepharose (in EBC) was incubated with 5 uL of 2.32 mg/mL Rabbit anti-Mouse IgG secondary antibody for 1 hour at 4°C to permit antibody binding to the Protein A beads. Following incubation, the beads were collected by centrifugation and washed three times with 200 uL of NET-N wash buffer, consisting of 20 mM Tris (pH 8.0), 100 mM NaCl, 1mM EDTA, and 0.5% NP40. Cell lysate (1 mg) and 20 uL of the SC-8050 (200 ug/mL) anti-ErbB4 mouse monoclonal antibody (Santa Cruz Biotechnologies, Santa Cruz, CA) were added and incubated for 2 hours at 4°C. Following incubation, the immunoprecipitates were washed three times with 500 uL of NET-N wash buffer. After washing, 80 uL of protein sample buffer containing 10% β-mercaptoethanol was added to the immunoprecipitates and samples were boiled for 5 minutes to release the precipitated antigen from the beads.

3.4.6.3. Immunoblotting and visualization

All samples were resolved by SDS-PAGE using a 7.5% acrylamide gel. Resolved samples were transferred from a gel to 0.2 uM PVDF (GE Healthcare - Life Sciences) using the Bio-Rad Trans-Blot Turbo Transfer System. Blots were probed using the

following primary antibodies: 4G10 antiphosphotyrosine mouse monoclonal antibody (Millipore, Billerica, MA), 4795S anti-ErbB4 rabbit monoclonal antibody (Cell Signaling, Danvers, MA), 4058S anti-phospho-Akt (Ser473) rabbit monoclonal antibody (Cell Signaling, Danvers, MA), 9272S anti-Akt rabbit polyclonal antibody (Cell Signaling, Danvers, MA), SC-7383 anti-phospho-Erk mouse monoclonal antibody (Santa Cruz Biotechnologies, Santa Cruz, CA), and SC-94 anti-Erk rabbit polyclonal antibody (Santa Cruz Biotechnologies, Santa Cruz, CA). Blots were then probed using either of the following secondary antibodies as appropriate: 31430 goat anti-mouse IgG (H+L) conjugated to HRP (ThermoFisher Scientific, Waltham, MA), or 31460 goat anti-rabbit IgG (H+L) conjugated to HRP (ThermoFisher Scientific, Waltham, MA). Antibody binding was visualized by chemiluminesence using a Bio-Rad Chemidoc MP imaging system.

3.5. Conclusions

In this work, reliable, reproducible, and scalable approaches were developed, validated, and deployed for the discovery of compounds that hold potential as targeted cancer therapeutics. Our drug discovery approach was based on the observation that the Q43L mutant of the naturally occurring ErbB4 agonist NRG2β functions as a partial agonist of ErbB4. NRG2β/Q43L stimulates ErbB4 tyrosine phosphorylation, fails to stimulate ErbB4-dependent cell proliferation, and inhibits agonist-induced ErbB4-dependent cell proliferation. ErbB4 partial agonists hold promise as therapies for ErbB4-dependent tumors. Using the screening assays developed in this work, six compounds were identified that stimulate ErbB4 tyrosine phosphorylation, fail to stimulate ErbB4-

dependent cell proliferation, and selectively inhibit ErbB4-dependent cell proliferation. While much work remains to further evaluate the therapeutic potential of these six compounds, this work has established a high-throughput screening process for the identification of ErbB4 inhibitors.

Chapter 4: Conclusions

Despite the major advancements that have been made in the treatment of metastatic melanoma, the survival rate of these patients remains unacceptable. Until the genetics behind the disease is better understood, it is unclear whether patient outcomes will improve. Fortunately, organizations like the National Institutes of Health's National Cancer Institute have led major cancer genome sequencing programs, such as The Cancer Genome Atlas (TCGA), to provide all cancer researchers with clinical genomic data for the development of precision oncology therapies. The work described in this dissertation is just one example of how these publicly available clinical genomic data sets can be used for cancer drug discovery.

Our analyses of the skin cutaneous melanoma (SKCM) clinical genomic data set created by the TCGA revealed that a significant fraction of melanomas harbor mutations in the gene that encodes for the ErbB4 receptor tyrosine kinase. Moreover, in-depth analyses of the nonsynonymous missense *ERBB4* mutations in the TCGA-SKCM data set suggests that many of the mutations are likely to function as drivers of melanoma cell proliferation. Therefore, there is a dire need to determine which *ERBB4* mutations contribute to the malignant phenotype of melanoma. Identifying which patients that would benefit from an anti-ErbB4 therapy has the potential to affect a significant portion of metastatic melanoma patients.

As such, it is critical to develop treatment strategies for patients that have ErbB4-dependent melanomas. Due to the biochemical and biological properties of ErbB4, molecules that function as ErbB4 partial agonists hold great therapeutic potential for ErbB4-dependent melanomas. Based on previous work, molecules that stimulate ErbB4 tyrosine phosphorylation, fail to stimulate ErbB4-dependent cell proliferation, and inhibit agonist-induced ErbB4-dependent cell proliferation are highly likely to function as ErbB4 partial agonists. Therefore, in this work, three highly sensitive and reproducible (Z' > 0.5) semi-automated assays were developed for the discovery of ErbB4 partial agonists that function as antagonists at ErbB4. When deployed, this screening process identified six small-molecule compounds (1 high priority and 5 medium priority candidates) that stimulate ErbB4 phosphorylation yet selectively inhibit ErbB4-dependent cell proliferation. These molecules are highly likely to function as ErbB4 partial agonists, and as such hold promise as targeted therapies for ErbB4-dependent melanomas.

Hopefully, the results of this work have exposed the therapeutic potential for a target that is currently not well understood in a disease that is facing major clinical problems. The insights made from the clinical genomic data in the TCGA-SKCM data set should serve as a platform for the discovery of *ERBB4* mutants that contribute to melanoma tumorigenesis. Additionally, the drug-discovery screening process that was developed and implemented in this work will serve as a foundation for the discovery of a new class of ErbB targeted therapies. Therapies that do not simply treat ErbB receptors as on/off switches; but, instead, utilize their differentiated signaling as an opportunity for novel mechanisms-of-action.

Chapter 5: Future Directions

5.1. Future directions for the identification of *ERBB4* driver mutations in melanoma

As discussed in Chapter 2, many of the *ERBB4* nonsynonymous missense mutations found in the TCGA-SKCM data set have the potential to function as drivers of melanoma cell proliferation. Therefore, we will use traditional molecular genetics and biological approaches to determine which of these mutations are necessary for the growth of melanoma cells. Furthermore, we will determine whether the mutants function as gain-of-function (GOF) or loss-of-function (LOF) in context of ErbB4 signaling.

5.1.1. Identify GOF *ERBB4* mutant alleles that function as drivers of melanoma cell proliferation

We will begin characterizing the highest prioritized mutations (**Table 5**) using traditional approaches for identifying GOF driver mutations in genes that encode for ErbB receptors. First, each of the *ERBB4* mutations and wild-type *ERBB4* will be transiently expressed in NIH 3T3 cells to determine whether they induce focus formation. A driver mutation will typically cause more focus formation than the wild-type gene. Next, we will use the same NIH 3T3 cell lines that contain the mutants and the wild-type gene to determine whether any of the mutations cause ligand-independent tyrosine phosphorylation. Mutations that are likely to be GOF drivers will exhibit increased ligand-independent tyrosine phosphorylation compared to the wild-type gene. However,

as mentioned in Chapter 3, the level of tyrosine phosphorylation is not necessarily indicative of biological response. Therefore, mutants that induce increased focus formation may not exhibit elevated ligand-independent tyrosine phosphorylation and mutants that do not induce increased focus formation may exhibit elevated ligand-independent tyrosine phosphorylation.

As such, each of the mutants will also be tested for whether or not they are necessary for the proliferation of an ErbB4-dependent melanoma cell line. Each of the 10 mutations will be stably expressed in the ErbB4-dependent 7T human melanoma cell line[26] which already contains the *ERBB4* E452K mutation. Then, we will use shRNA that silences the endogenous *ERBB4* but not the ectopic *ERBB4*. Mutations that are necessary for ErbB4-dependent cell proliferation will render the 7T cells resistant to the *ERBB4* shRNA that silenced the endogenous *ERBB4* and rescue 7T cell proliferation. Furthermore, *ERBB4* mutations that rescue 7T cell proliferation are highly likely to function as drivers of ErbB4-dependent melanoma tumorigenesis and serve as biomarkers for therapies that disrupt ErbB4 signaling.

Additionally, completing these experiments will establish a process for characterizing *ERBB4* mutants in melanoma. Therefore, it will be possible to go back and characterize the remainder of the 71 *ERBB4* mutations in the TCGA-SKCM data set; many of which are likely to function as GOF drivers in melanoma.

5.1.2. Identify LOF *ERBB4* mutant alleles that likely function as drivers of melanoma cell proliferation

As discussed earlier, the proliferation of BaF3 cells are dependent on IL3. Since ErbB4 homodimers function as tumor suppressors, ligand stimulation of ErbB4 homodimers in BaF3 cells that express ErbB4 will inhibit the proliferation stimulated by IL3. Therefore, we will use BaF3 cells that ectopically express ErbB4 to identify LOF *ERBB4* mutant alleles that permit IL3-dependent cell proliferation in the presence of an ErbB4 ligand.

BaF3 cells will be infected with *ERBB4* mutant retroviruses containing the highly prioritized mutants in **Table 5**. The BaF3/*ERBB4* mutant cells will then be seeded and grown in the presence of IL3 and a saturating concentration of the ErbB4 agonist NRG1β until the cells reach saturation density. This process will select for *ERBB4* mutant alleles that disrupt the ErbB4 homodimer's ability to suppress cell proliferation and are likely to function as melanoma tumor suppressors

5.2. Future directions for the putative ErbB4 partial agonists

5.2.1. Evaluate the therapeutic potential of candidate inhibitors against ErbB4-dependent melanoma cell lines

While further characterizing the mechanism of action of the six candidate ErbB4 partial agonists is necessary for the advancement of these molecules, it would be interesting to see whether they could inhibit the proliferation of an ErbB4-dependent melanoma cell line. They each have shown inhibitory effects against an ErbB4-dependent model cell system but have not been tested in an ErbB4-dependent cancer cell line.

The ErbB4-dependent human melanoma cell line[26] could be used to determine whether these 6 molecules can inhibit ErbB4-dependent melanoma cell proliferation. Briefly, 7T cells and melanoma cells that are not ErbB4-dependent would be aseptically seeded in complete culture medium in a 24-well plate and dosed with increasing concentrations of each of the 6 candidate ErbB4 partial agonists. An MTT assay could then be performed to measure cell proliferation in the presence or absence of each of the compounds. For compounds that inhibit ErbB4-dependent melanoma cell proliferation, 7T cell proliferation should decrease as the concentration of compound increases. Furthermore, the non-ErbB4-dependent melanoma cell line proliferation should either remain unaffected by increasing concentrations of compound or cell proliferation should begin to decrease at much higher concentrations of compound than observed in the 7T cell line. A significant rightward shift (decrease in inhibitor potency) in the inhibitory dose response would still be indicative of selective inhibition of ErbB4-dependent melanoma cell proliferation.

5.2.2. Screen for monoclonal antibodies that function as ErbB4 partial agonists

In addition to discovering small-molecules that function as ErbB4 partial agonists, we could also use the semi-automated screening process described in Chapter 3 to identify monoclonal antibodies that are likely to function as ErbB4 partial agonists. It is possible that the potencies of the lead small-molecules cannot be improved using traditional medicinal chemistry approaches such that they can be used at clinically tolerable concentrations. Or, it is possible that none of the candidate small-molecules can inhibit the proliferation of ErbB4-dependent melanoma cells. In that case, screening a

library of monoclonal antibodies that were produced in response to fragments of ErbB4 would be a plausible next step. Although the cost of producing a monoclonal antibody library is significant, this is a proven method for the development of FDA-approved targeted therapies for ErbB receptors[72].

After the creation of the monoclonal antibody library, the screening process would be deployed as described in Chapter 3 for the identification of antibodies that function as partial agonists; and, therefore, hold potential as therapies against ErbB4-dependent melanomas.

References

1. Kuske, M.; Westphal, D.; Wehner, R.; Schmitz, M.; Beissert, S.; Praetorius, C.; Meier, F. Immunomodulatory effects of BRAF and MEK inhibitors: Implications for Melanoma therapy. *Pharmacol Res* **2018**, *136*, 151-159, doi:10.1016/j.phrs.2018.08.019.

2. Long, G.V.; Eroglu, Z.; Infante, J.; Patel, S.; Daud, A.; Johnson, D.B.; Gonzalez, R.; Kefford, R.; Hamid, O.; Schuchter, L., et al. Long-Term Outcomes in Patients With BRAF V600-Mutant Metastatic Melanoma Who Received Dabrafenib Combined With Trametinib. *J Clin Oncol* **2018**, *36*, 667-673, doi:10.1200/JCO.2017.74.1025.

3. Long, G.V.; Grob, J.J.; Nathan, P.; Ribas, A.; Robert, C.; Schadendorf, D.; Lane, S.R.; Mak, C.; Legenne, P.; Flaherty, K.T., et al. Factors predictive of response, disease progression, and overall survival after dabrafenib and trametinib combination treatment: a pooled analysis of individual patient data from randomised trials. *Lancet Oncol* **2016**, *17*, 1743-1754, doi:10.1016/S1470-2045(16)30578-2.

4. Hamid, O.; Robert, C.; Daud, A.; Hodi, F.S.; Hwu, W.J.; Kefford, R.; Wolchok, J.D.; Hersey, P.; Joseph, R.; Weber, J.S., et al. Five-year survival outcomes for patients with advanced melanoma treated with pembrolizumab in KEYNOTE-001. *Ann Oncol* **2019**, *30*, 582-588, doi:10.1093/annonc/mdz011.

5. Robert, C.; Schachter, J.; Long, G.V.; Arance, A.; Grob, J.J.; Mortier, L.; Daud, A.; Carlino, M.S.; McNeil, C.; Lotem, M., et al. Pembrolizumab versus Ipilimumab in Advanced Melanoma. *N Engl J Med* **2015**, *372*, 2521-2532, doi:10.1056/NEJMoa1503093.

6. Larkin, J.; Chiarion-Sileni, V.; Gonzalez, R.; Grob, J.J.; Rutkowski, P.; Lao, C.D.; Cowey, C.L.; Schadendorf, D.; Wagstaff, J.; Dummer, R., et al. Five-Year Survival with Combined Nivolumab and Ipilimumab in Advanced Melanoma. *N Engl J Med* **2019**, *381*, 1535-1546, doi:10.1056/NEJMoa1910836.

7. Wolchok, J.D.; Chiarion-Sileni, V.; Gonzalez, R.; Rutkowski, P.; Grob, J.J.; Cowey, C.L.; Lao, C.D.; Wagstaff, J.; Schadendorf, D.; Ferrucci, P.F., et al. Overall Survival with Combined Nivolumab and Ipilimumab in Advanced Melanoma. *N Engl J Med* **2017**, *377*, 1345-1356, doi:10.1056/NEJMoa1709684.

8. NCI. SEER Cancer Stat Facts: Melanoma of the Skin. Availabe online: https://seer.cancer.gov/statfacts/html/melan.html (accessed on October 2 2018).

9. Najem, A.; Krayem, M.; Perdrix, A.; Kerger, J.; Awada, A.; Journe, F.; Ghanem, G. New Drug Combination Strategies in Melanoma: Current Status and Future Directions. *Anticancer Res* **2017**, *37*, 5941-5953, doi:10.21873/anticanres.12041.

10. Bollag, G.; Tsai, J.; Zhang, J.; Zhang, C.; Ibrahim, P.; Nolop, K.; Hirth, P. Vemurafenib: the first drug approved for BRAF-mutant cancer. *Nat Rev Drug Discov* **2012**, *11*, 873-886, doi:10.1038/nrd3847.

11. Chapman, P.B.; Hauschild, A.; Robert, C.; Haanen, J.B.; Ascierto, P.; Larkin, J.; Dummer, R.; Garbe, C.; Testori, A.; Maio, M., et al. Improved survival with vemurafenib in melanoma with BRAF V600E mutation. *N Engl J Med* **2011**, *364*, 2507-2516, doi:10.1056/NEJMoa1103782.

12. Flaherty, K.T.; Robert, C.; Hersey, P.; Nathan, P.; Garbe, C.; Milhem, M.; Demidov, L.V.; Hassel, J.C.; Rutkowski, P.; Mohr, P., et al. Improved survival with MEK inhibition in BRAF-mutated melanoma. *N Engl J Med* **2012**, *367*, 107-114, doi:10.1056/NEJMoa1203421.

13. Niezgoda, A.; Niezgoda, P.; Czajkowski, R. Novel Approaches to Treatment of Advanced Melanoma: A Review on Targeted Therapy and Immunotherapy. *Biomed Res Int* **2015**, *2015*, 851387, doi:10.1155/2015/851387.

14. Daud, A. Current and Emerging Perspectives on Immunotherapy for Melanoma. *Semin Oncol* **2015**, *42 Suppl 3*, S3-S11, doi:10.1053/j.seminoncol.2015.10.003.

15. Grossman, R.L.; Heath, A.P.; Ferretti, V.; Varmus, H.E.; Lowy, D.R.; Kibbe, W.A.; Staudt, L.M. Toward a Shared Vision for Cancer Genomic Data. *N Engl J Med* **2016**, *375*, 1109-1112, doi:10.1056/NEJMp1607591.

16. Cerami, E.; Gao, J.; Dogrusoz, U.; Gross, B.E.; Sumer, S.O.; Aksoy, B.A.; Jacobsen, A.; Byrne, C.J.; Heuer, M.L.; Larsson, E., et al. The cBio cancer genomics portal: an open platform for exploring multidimensional cancer genomics data. *Cancer Discov* **2012**, *2*, 401-404, doi:10.1158/2159-8290.CD-12-0095.

17. Gao, J.; Aksoy, B.A.; Dogrusoz, U.; Dresdner, G.; Gross, B.; Sumer, S.O.; Sun, Y.; Jacobsen, A.; Sinha, R.; Larsson, E., et al. Integrative analysis of complex cancer genomics and clinical profiles using the cBioPortal. *Sci Signal* **2013**, *6*, pl1, doi:10.1126/scisignal.2004088.

18. Chen, B.; Butte, A.J. Leveraging big data to transform target selection and drug discovery. *Clin Pharmacol Ther* **2016**, *99*, 285-297, doi:10.1002/cpt.318.

19. Davies, H.; Bignell, G.R.; Cox, C.; Stephens, P.; Edkins, S.; Clegg, S.; Teague, J.; Woffendin, H.; Garnett, M.J.; Bottomley, W., et al. Mutations of the BRAF gene in human cancer. *Nature* **2002**, *417*, 949-954, doi:10.1038/nature00766.

20. Flaherty, K.T.; Puzanov, I.; Kim, K.B.; Ribas, A.; McArthur, G.A.; Sosman, J.A.; O'Dwyer, P.J.; Lee, R.J.; Grippo, J.F.; Nolop, K., et al. Inhibition of mutated, activated BRAF in metastatic melanoma. *N Engl J Med* **2010**, *363*, 809-819, doi:10.1056/NEJMoa1002011.

21. de Silva, C.M.; Reid, R. Gastrointestinal stromal tumors (GIST): C-kit mutations, CD117 expression, differential diagnosis and targeted cancer therapy with Imatinib. *Pathol Oncol Res* **2003**, *9*, 13-19, doi:PAOR.2003.9.1.0013.

22. Macarron, R.; Banks, M.N.; Bojanic, D.; Burns, D.J.; Cirovic, D.A.; Garyantes, T.; Green, D.V.; Hertzberg, R.P.; Janzen, W.P.; Paslay, J.W., et al. Impact of high-throughput screening in biomedical research. *Nat Rev Drug Discov* **2011**, *10*, 188-195, doi:10.1038/nrd3368.

23. Hoelder, S.; Clarke, P.A.; Workman, P. Discovery of small molecule cancer drugs: successes, challenges and opportunities. *Mol Oncol* **2012**, *6*, 155-176, doi:10.1016/j.molonc.2012.02.004.

24. An, W.F.; Tolliday, N. Cell-based assays for high-throughput screening. *Mol Biotechnol* **2010**, *45*, 180-186, doi:10.1007/s12033-010-9251-z.

25. CHEN Fact Sheet. Auburn University: 2018.

26. Prickett, T.D.; Agrawal, N.S.; Wei, X.; Yates, K.E.; Lin, J.C.; Wunderlich, J.R.; Cronin, J.C.; Cruz, P.; Rosenberg, S.A.; Samuels, Y. Analysis of the tyrosine kinome in melanoma reveals recurrent mutations in ERBB4. *Nat Genet* **2009**, *41*, 1127-1132, doi:10.1038/ng.438.

27. Sjoblom, T.; Jones, S.; Wood, L.D.; Parsons, D.W.; Lin, J.; Barber, T.D.; Mandelker, D.; Leary, R.J.; Ptak, J.; Silliman, N., et al. The consensus coding sequences of human breast and colorectal cancers. *Science* **2006**, *314*, 268-274, doi:10.1126/science.1133427.

28. Cancer Genome Atlas, N. Genomic Classification of Cutaneous Melanoma. *Cell* **2015**, *161*, 1681-1696, doi:10.1016/j.cell.2015.05.044.

29. Lee, J.C.; Vivanco, I.; Beroukhim, R.; Huang, J.H.; Feng, W.L.; DeBiasi, R.M.; Yoshimoto, K.; King, J.C.; Nghiemphu, P.; Yuza, Y., et al. Epidermal growth factor receptor activation in glioblastoma through novel missense mutations in the extracellular domain. *PLoS Med* **2006**, *3*, e485, doi:10.1371/journal.pmed.0030485.

30. Brennan, C.W.; Verhaak, R.G.; McKenna, A.; Campos, B.; Noushmehr, H.; Salama, S.R.; Zheng, S.; Chakravarty, D.; Sanborn, J.Z.; Berman, S.H., et al. The somatic genomic landscape of glioblastoma. *Cell* **2013**, *155*, 462-477, doi:10.1016/j.cell.2013.09.034.

31. Boulbes, D.R.; Arold, S.T.; Chauhan, G.B.; Blachno, K.V.; Deng, N.; Chang, W.C.; Jin, Q.; Huang, T.H.; Hsu, J.M.; Brady, S.W., et al. HER family kinase domain mutations promote tumor progression and can predict response to treatment in human breast cancer. *Mol Oncol* **2015**, *9*, 586-600, doi:10.1016/j.molonc.2014.10.011.

32. Cai, C.Q.; Peng, Y.; Buckley, M.T.; Wei, J.; Chen, F.; Liebes, L.; Gerald, W.L.; Pincus, M.R.; Osman, I.; Lee, P. Epidermal growth factor receptor activation in prostate cancer by three novel missense mutations. *Oncogene* **2008**, *27*, 3201-3210, doi:10.1038/sj.onc.1210983.

33. Li, M.; Zhang, Z.; Li, X.; Ye, J.; Wu, X.; Tan, Z.; Liu, C.; Shen, B.; Wang, X.A.; Wu, W., et al. Whole-exome and targeted gene sequencing of gallbladder carcinoma identifies recurrent mutations in the ErbB pathway. *Nat Genet* **2014**, *46*, 872-876, doi:10.1038/ng.3030.

34. Lynch, T.J.; Bell, D.W.; Sordella, R.; Gurubhagavatula, S.; Okimoto, R.A.; Brannigan, B.W.; Harris, P.L.; Haserlat, S.M.; Supko, J.G.; Haluska, F.G., et al. Activating mutations in the epidermal growth factor receptor underlying responsiveness of non-small-cell lung cancer to gefitinib. *N Engl J Med* **2004**, *350*, 2129-2139, doi:10.1056/NEJMoa040938.

35. Pao, W.; Miller, V.; Zakowski, M.; Doherty, J.; Politi, K.; Sarkaria, I.; Singh, B.; Heelan, R.; Rusch, V.; Fulton, L., et al. EGF receptor gene mutations are common in lung cancers from "never smokers" and are associated with sensitivity of tumors to gefitinib and erlotinib. *Proc Natl Acad Sci U S A* **2004**, *101*, 13306-13311, doi:10.1073/pnas.0405220101.

36. Paez, J.G.; Janne, P.A.; Lee, J.C.; Tracy, S.; Greulich, H.; Gabriel, S.; Herman, P.; Kaye, F.J.; Lindeman, N.; Boggon, T.J., et al. EGFR mutations in lung cancer: correlation with clinical response to gefitinib therapy. *Science* **2004**, *304*, 1497-1500, doi:10.1126/science.1099314.

37. U, M.; Talevich, E.; Katiyar, S.; Rasheed, K.; Kannan, N. Prediction and prioritization of rare oncogenic mutations in the cancer Kinome using novel features and multiple classifiers. *PLoS Comput Biol* **2014**, *10*, e1003545, doi:10.1371/journal.pcbi.1003545.

38. Trowe, T.; Boukouvala, S.; Calkins, K.; Cutler, R.E., Jr.; Fong, R.; Funke, R.; Gendreau, S.B.; Kim, Y.D.; Miller, N.; Woolfrey, J.R., et al. EXEL-7647 inhibits mutant forms of ErbB2 associated with lapatinib resistance and neoplastic

transformation. *Clin Cancer Res* **2008**, *14*, 2465-2475, doi:10.1158/1078-0432.CCR-07-4367.

39. Kavuri, S.M.; Jain, N.; Galimi, F.; Cottino, F.; Leto, S.M.; Migliardi, G.; Searleman, A.C.; Shen, W.; Monsey, J.; Trusolino, L., et al. HER2 activating mutations are targets for colorectal cancer treatment. *Cancer Discov* **2015**, *5*, 832-841, doi:10.1158/2159-8290.CD-14-1211.

40. Yarden, Y.; Sliwkowski, M.X. Untangling the ErbB signalling network. *Nat Rev Mol Cell Biol* **2001**, *2*, 127-137, doi:10.1038/35052073.

41. Prior, I.A.; Lewis, P.D.; Mattos, C. A comprehensive survey of Ras mutations in cancer. *Cancer Res* **2012**, *72*, 2457-2467, doi:10.1158/0008-5472.CAN-11-2612.

42. Kiuru, M.; Busam, K.J. The NF1 gene in tumor syndromes and melanoma. *Lab Invest* **2017**, *97*, 146-157, doi:10.1038/labinvest.2016.142.

43. Wu, H.; Goel, V.; Haluska, F.G. PTEN signaling pathways in melanoma. *Oncogene* **2003**, *22*, 3113-3122, doi:10.1038/sj.onc.1206451.

44. Riese, D.J., 2nd; Komurasaki, T.; Plowman, G.D.; Stern, D.F. Activation of ErbB4 by the bifunctional epidermal growth factor family hormone epiregulin is regulated by ErbB2. *J Biol Chem* **1998**, *273*, 11288-11294.

45. Mill, C.P.; Zordan, M.D.; Rothenberg, S.M.; Settleman, J.; Leary, J.F.; Riese, D.J., 2nd. ErbB2 Is Necessary for ErbB4 Ligands to Stimulate Oncogenic Activities in Models of Human Breast Cancer. *Genes Cancer* **2011**, *2*, 792-804, doi:10.1177/1947601911431080.

46. Mill, C.P.; Gettinger, K.L.; Riese, D.J., 2nd. Ligand stimulation of ErbB4 and a constitutively-active ErbB4 mutant result in different biological responses in human pancreatic tumor cell lines. *Exp Cell Res* **2011**, *317*, 392-404, doi:10.1016/j.yexcr.2010.11.007.

47. Gallo, R.M.; Bryant, I.N.; Mill, C.P.; Kaverman, S.; Riese, D.J., 2nd. Multiple Functional Motifs Are Required for the Tumor Suppressor Activity of a Constitutively-Active ErbB4 Mutant. *J Cancer Res Ther Oncol* **2013**, *1*, 10.

48. Wilson, K.J.; Mill, C.P.; Gallo, R.M.; Cameron, E.M.; VanBrocklin, H.; Settleman, J.; Riese, D.J. The Q43L mutant of neuregulin 2beta is a pan-ErbB receptor antagonist. *Biochem J* **2012**, *443*, 133-144, doi:10.1042/BJ20110921.

49. Williams, E.E.; Trout, L.J.; Gallo, R.M.; Pitfield, S.E.; Bryant, I.; Penington, D.J.; Riese, D.J., 2nd. A constitutively active ErbB4 mutant inhibits drug-resistant colony formation by the DU-145 and PC-3 human prostate tumor cell lines. *Cancer Lett* **2003**, *192*, 67-74.

50. Riese, D.J., 2nd; Bermingham, Y.; van Raaij, T.M.; Buckley, S.; Plowman, G.D.; Stern, D.F. Betacellulin activates the epidermal growth factor receptor and erbB-4, and induces cellular response patterns distinct from those stimulated by epidermal growth factor or neuregulin-beta. *Oncogene* **1996**, *12*, 345-353.

51. Riese, D.J., 2nd; van Raaij, T.M.; Plowman, G.D.; Andrews, G.C.; Stern, D.F. The cellular response to neuregulins is governed by complex interactions of the erbB receptor family. *Mol Cell Biol* **1995**, *15*, 5770-5776.

52. Penington, D.J.; Bryant, I.; Riese, D.J., 2nd. Constitutively active ErbB4 and ErbB2 mutants exhibit distinct biological activities. *Cell Growth Differ* **2002**, *13*, 247-256.

53. Gallo, R.M.; Bryant, I.; Fry, R.; Williams, E.E.; Riese, D.J., 2nd. Phosphorylation of ErbB4 on Tyr1056 is critical for inhibition of colony formation by prostate tumor cell lines. *Biochem Biophys Res Commun* **2006**, *349*, 372-382, doi:10.1016/j.bbrc.2006.08.055.

54. Pitfield, S.E.; Bryant, I.; Penington, D.J.; Park, G.; Riese, D.J., 2nd. Phosphorylation of ErbB4 on tyrosine 1056 is critical for ErbB4 coupling to inhibition of colony formation by human mammary cell lines. *Oncol Res* **2006**, *16*, 179-193, doi:10.3727/000000006783981134.

55. Hamid, O.; Robert, C.; Daud, A.; Hodi, F.S.; Hwu, W.J.; Kefford, R.; Wolchok, J.D.; Hersey, P.; Joseph, R.; Weber, J.S., et al. Five-year survival outcomes for patients with advanced melanoma treated with pembrolizumab in KEYNOTE-001. *Ann Oncol* **2019**, 10.1093/annonc/mdz011, doi:10.1093/annonc/mdz011.

56. Cullum, R.L.; Lucas, L.; Ghosh, T.; Riese, D.J., 2nd. Unpublished results.

57. Hobbs, S.S.; Coffing, S.L.; Le, A.T.; Cameron, E.M.; Williams, E.E.; Andrew, M.; Blommel, E.N.; Hammer, R.P.; Chang, H.; Riese, D.J., 2nd. Neuregulin isoforms exhibit distinct patterns of ErbB family receptor activation. *Oncogene* **2002**, *21*, 8442-8452, doi:10.1038/sj.onc.1205960.

58. Riese, D.J.; Kim, E.D.; Elenius, K.; Buckley, S.; Klagsbrun, M.; Plowman, G.D.; Stern, D.F. The epidermal growth factor receptor couples transforming growth factor-alpha, heparin-binding epidermal growth factor-like factor, and amphiregulin to Neu, ErbB-3, and ErbB-4. *J Biol Chem* **1996**, *271*, 20047-20052.

59. Hobbs, S.S.; Cameron, E.M.; Hammer, R.P.; Le, A.T.; Gallo, R.M.; Blommel, E.N.; Coffing, S.L.; Chang, H.; Riese, D.J., 2nd. Five carboxyl-terminal residues of neuregulin2 are critical for stimulation of signaling by the ErbB4 receptor tyrosine kinase. *Oncogene* **2004**, *23*, 883-893, doi:10.1038/sj.onc.1207250.

60. Wu, P.; Nielsen, T.E.; Clausen, M.H. FDA-approved small-molecule kinase inhibitors. *Trends Pharmacol Sci* **2015**, *36*, 422-439, doi:10.1016/j.tips.2015.04.005.

61. Arteaga, C.L.; Engelman, J.A. ERBB receptors: from oncogene discovery to basic science to mechanism-based cancer therapeutics. *Cancer Cell* **2014**, *25*, 282-303, doi:10.1016/j.ccr.2014.02.025.

62. Hynes, N.E.; Lane, H.A. ERBB receptors and cancer: the complexity of targeted inhibitors. *Nat Rev Cancer* **2005**, *5*, 341-354, doi:10.1038/nrc1609.

63. Plowman, G.D.; Green, J.M.; Culouscou, J.M.; Carlton, G.W.; Rothwell, V.M.; Buckley, S. Heregulin induces tyrosine phosphorylation of HER4/p180erbB4. *Nature* **1993**, *366*, 473-475, doi:10.1038/366473a0.

64. Engvall, E.; Perlmann, P. Enzyme-linked immunosorbent assay (ELISA). Quantitative assay of immunoglobulin G. *Immunochemistry* **1971**, *8*, 871-874.

65. Zhang, J.H.; Chung, T.D.; Oldenburg, K.R. A Simple Statistical Parameter for Use in Evaluation and Validation of High Throughput Screening Assays. *J Biomol Screen* **1999**, *4*, 67-73, doi:10.1177/108705719900400206.

66. Mosmann, T. Rapid colorimetric assay for cellular growth and survival: application to proliferation and cytotoxicity assays. *J Immunol Methods* **1983**, *65*, 55-63.

67. Hennequin, L.F.; Ballard, P.; Boyle, F.T.; Delouvrie, B.; Ellston, R.P.; Halsall, C.T.; Harris, C.S.; Hudson, K.; Kendrew, J.; Pease, J.E., et al. Novel 4-anilinoquinazolines with C-6 carbon-linked side chains: synthesis and structure-activity relationship of a series of potent, orally active, EGF receptor tyrosine kinase inhibitors. *Bioorg Med Chem Lett* **2006**, *16*, 2672-2676, doi:10.1016/j.bmcl.2006.02.025.

68. Wakeling, A.E.; Guy, S.P.; Woodburn, J.R.; Ashton, S.E.; Curry, B.J.; Barker, A.J.; Gibson, K.H. ZD1839 (Iressa): an orally active inhibitor of epidermal growth factor signaling with potential for cancer therapy. *Cancer Res* **2002**, *62*, 5749-5754.

69. Rowinsky, E. The Vinca Alkaloids. In *Holland-Frei Cancer Medicine. 6th edition.* , BC Decker: Hamilton (ON), 2003.

70. Kaushansky, A.; Gordus, A.; Budnik, B.A.; Lane, W.S.; Rush, J.; MacBeath, G. System-wide investigation of ErbB4 reveals 19 sites of Tyr phosphorylation that are unusually selective in their recruitment properties. *Chem Biol* **2008**, *15*, 808-817, doi:10.1016/j.chembiol.2008.07.006.

71. Wilson, K.J.; Mill, C.P.; Cameron, E.M.; Hobbs, S.S.; Hammer, R.P.; Riese, D.J., 2nd. Inter-conversion of neuregulin2 full and partial agonists for ErbB4. *Biochem Biophys Res Commun* **2007**, *364*, 351-357, doi:10.1016/j.bbrc.2007.10.004.

72. Schmitz, K.R.; Ferguson, K.M. Interaction of antibodies with ErbB receptor extracellular regions. *Exp Cell Res* **2009**, *315*, 659-670, doi:10.1016/j.yexcr.2008.10.008.